Remote Sensing of Environment 115 (2011) 3203–3219

Contents lists available at ScienceDirect

Remote Sensing of Environment

journal homepage: www.elsevier.com/locate/rse

Snow-covered Landsat time series stacks improve automated disturbance mapping accuracy in forested landscapes

Kirk M. Stueve [a,*], Ian W. Housman [b], Patrick L. Zimmerman [a], Mark D. Nelson [a], Jeremy B. Webb [b], Charles H. Perry [a], Robert A. Chastain [b], Dale D. Gormanson [a], Chengquan Huang [c], Sean P. Healey [d], Warren B. Cohen [e]

[a] United States Department of Agriculture Forest Service, Northern Research Station, Forest Inventory and Analysis, 1992 Folwell Avenue, Saint Paul, MN 55108, USA
[b] United States Department of Agriculture Forest Service, Remote Sensing Applications Center, 2222 West 2300 South, Salt Lake City, UT 84119, USA
[c] University of Maryland, Department of Geography, 2181A LeFrak Hall, College Park, MD 20742 USA
[d] United States Department of Agriculture Forest Service, Rocky Mountain Research Station, Forest Inventory and Analysis, 507 25th Street, Ogden, UT 84401, USA
[e] United States Department of Agriculture Forest Service, Pacific Northwest Research Station, Forest Inventory and Analysis, 3200 SW Jefferson Way, Corvallis, OR 97331, USA

ARTICLE INFO

Article history:
Received 7 May 2011
Received in revised form 5 July 2011
Accepted 7 July 2011
Available online 11 August 2011

Keywords:
Automated disturbance mapping
Eastern deciduous forest
Forest disturbance commission errors
Landsat time series stacks
Great Lakes
Mixed northern hardwoods
Satellite remote sensing
Snow
Southern boreal forest
Validation
Vegetation change tracker
Winter

ABSTRACT

Accurate landscape-scale maps of forests and associated disturbances are critical to augment studies on biodiversity, ecosystem services, and the carbon cycle, especially in terms of understanding how the spatial and temporal complexities of damage sustained from disturbances influence forest structure and function. Vegetation change tracker (VCT) is a highly automated algorithm that exploits the spectral–temporal properties of summer Landsat time series stacks (LTSSs) to generate spatially explicit maps of forest and recent forest disturbances. VCT performs well in contiguous forest landscapes with closed or nearly closed canopies, but often incorrectly classifies large patches of land as forest or forest disturbance in the complex and spatially heterogeneous environments that typify fragmented forest landscapes. We introduce an improved version of VCT (dubbed VCTw) that incorporates a nonforest mask derived from snow-covered winter Landsat time series stacks (LTSSw) and compare it with VCT across nearly 25 million ha of land in the Lake Superior (Canada, USA) and Lake Michigan (USA) drainage basins.

Accuracy assessments relying on 87 primary sampling units (PSUs) and 2640 secondary sampling units (SSUs) indicated that VCT performed with an overall accuracy of 86.3%. For persisting forest, the commission error was 14.7% and the omission error was 4.3%. Commission and omission errors for the two forest disturbance classes fluctuated around 50%. VCTw produced a statistically significant increase in overall accuracy to 91.2% and denoted about 1.115 million ha less forest (−.371 million ha disturbed and −0.744 million ha persisting). For persisting forest, the commission error decreased to 9.3% and the omission error was relatively unchanged at 5.0%. Commission errors decreased considerably to near 22% and omission errors remained near 50% in both forest disturbance classes.

Dividing the assessments into three geographic strata demonstrated that the most dramatic improvement occurred across the southern half of the Lake Michigan basin, which contains a highly fragmented agricultural landscape and relatively sparse deciduous forest, although substantial improvements occurred in other geographic strata containing little agricultural land, abundant wetlands, and extensive coniferous forest. Unlike VCT, VCTw also generally corresponded well with field-based estimates of forest cover in each stratum. Snow-covered winter imagery appears to be a valuable resource for improving automated disturbance mapping accuracy. About 34% of the world's forests receive sufficient snowfall to cover the ground and are potentially suitable for VCTw; other season-based techniques may be worth pursuing for the remaining 66%.

Published by Elsevier Inc.

1. Introduction

Forests are vital for maintaining biodiversity (Myers et al., 2000) and providing invaluable ecosystem services (Costanza et al., 1997). In forested landscapes, natural and anthropogenic disturbances are fundamental mechanisms of change that exert significant influences on forest structure and function across a range of spatial and temporal scales (Foster et al., 1998; Schulte et al., 2007, Stueve et al., 2009; Stueve et al., 2011; Turner, 2005; Woods, 2004). Tree canopy damage patterns from landscape-scale disturbances, in particular, tend to be patchy and highly variable, controlled by the complexities of cascading interactions between the spatial heterogeneity of landscape

* Corresponding author at: 1992 Folwell Avenue, Saint Paul, MN 55108, USA. Tel.: +1 651 649 5025; fax: +1 651 649 5140.
E-mail address: kstueve@biogeography.us (K.M. Stueve).

0034-4257/$ – see front matter. Published by Elsevier Inc.
doi:10.1016/j.rse.2011.07.005

features and disturbances themselves (Flatley et al., 2011; Nelson et al., 2009; Rich et al., 2010; Stueve et al., 2007). For example, trees are more susceptible to ice and wind damage near the forest edge (Millward et al., 2010; Stueve et al., 2011), but damage may also be more extensive and severe near a particularly intense part of a storm irrespective of forest edge. Furthermore, the presence of forest edge is dependent on the spatial distribution and damage severity of other natural and anthropogenic stand-clearing disturbances. Damage patterns from anthropogenic disturbances, such as forest harvest, are also spatially heterogeneous and tend to favor easily accessible stands comprising high quality timber, salvageable stands recently damaged by natural disturbances, and private lands in general (Kittredge et al., 2003; Schmiegelow et al., 2006). Indeed, it is of paramount importance to identify and contextualize these interrelationships in order to increase our understanding of forest ecosystems and their interactions with other systems.

The implications of spatially heterogeneous patterns and processes in forested landscapes on the photosynthetic uptake of carbon, in particular, have received considerable attention in the midst of rapidly rising atmospheric carbon dioxide (CO_2) levels and ongoing climate change (Dixon et al., 1994; Goodale et al., 2002; Goward et al., 2008). Forests usually release carbon after a major disturbance because of increased respiration from decomposers and only transition to carbon sinks when photosynthetic carbon uptake from regrowing trees exceeds the release from decomposers (Goward et al., 2008; Rice et al., 2004). However, the heterogeneous nature of forests and persistent state of flux would allow, for example, two neighboring stands to act as a carbon source and sink respectively, or a rapid disturbance-facilitated shift from a stand that sequesters carbon to one that releases it (Goodale et al., 2002; Goward et al., 2008; Kurz et al., 2008). Current systematic sampling schemes of field-based research plots cannot reliably detect all of these spatially and temporally heterogeneous events, and ultimately they do not provide a sufficient understanding of ecological pattern and process at landscape-scales (e.g., spatially explicit patterns and processes across thousands of hectares or more). For example, Stueve et al. (2011) could not rely on United States Department of Agriculture (USDA) Forest Service, Forest Inventory and Analysis (FIA) plot data for validating ~50,000 ha of forest damage from four windstorms in the northern Great Lakes because the patchy damage patterns affected few FIA sample plots, and the timing of two storms preceded established sampling intervals. Indeed, problems arising from the aforementioned examples and others (e.g., Nelson et al., 2009) have introduced unacceptable uncertainty levels (estimated as low as 8–25% and upwards to 50%) in North American estimates of carbon flux (Heath et al., 2011; c.f. Thomas et al., 2011) and will present challenges to acquiring reliable estimates across the globe (Goodale et al., 2002). Not surprisingly, there is a burgeoning consensus among ecologists that spatially explicit and temporally dense forest disturbance and regrowth data encompassing large spatial extents are essential for developing an improved understanding of complex ecological phenomena in forests.

Fortunately, the recent accomplishments and future interests of remote sensing scientists and ecologists appear to be rapidly converging (Rich et al., 2010), and the remote sensing community is poised to provide an abundance of invaluable data at landscape scales to fulfill the expanding needs of ecologists (Huang et al., 2010a; Kennedy et al., 2010). Passive satellite remote sensing platforms in the visible and near infrared (VNIR) and shortwave infrared (SWIR) ranges of the electromagnetic spectrum are well-suited for these purposes because of their typically dense temporal coverage spanning the last several decades, moderate spatial resolutions, and comprehensive global coverage (Epting et al., 2005; Goward et al., 2006; Jakubauskas, 1996; Soverel et al., 2010). Until recently, most disturbance mapping and change detection approaches only utilized imagery with limited temporal coverage (Lu et al., 2004; Singh, 1989). These coarse temporal sequences (often bi-temporal, e.g., decadal) are undoubtedly useful, but they are ineffective at capturing the broad array of patchy and spatially explicit natural and anthropogenic changes frequently occurring on forested landscapes (Lambin, 1996). Such approaches also may lack temporal frequency sufficient to detect more rapid instances of disturbance and recovery. However, over the last approximately five years, great conceptual and technological achievements have been realized in developing practical and efficient approaches for creating and validating dense temporal assessments of forest disturbance and regrowth (Chuvieco et al., 2005; Cohen et al., 2010; Huang et al., 2010a; Jin & Sader, 2005; Kennedy et al., 2007, 2010; Thomas et al., 2011; Verbesselt et al., 2010). In the broader context, perhaps the most important recent development has been the free release of the entire Landsat archive, allowing for financially unconstrained acquisitions of dense temporal data stacks across large geographic extents.

Some of the most promising multitemporal approaches exploit the rich archive of Landsat satellite data (Cohen & Goward, 2004), which provides synoptic coverage of global forests over the last several decades at a moderately fine spatial resolution. Vegetation change tracker (VCT) (Huang et al., 2010a) and Landsat-based detection of trends in disturbance and regrowth (LandTrendr; Kennedy et al., 2010) are automated multitemporal approaches for detecting forest disturbance and regrowth patterns that rely on tracking pixel-by-pixel spectral trajectories of land surface changes over time in dense biennial or annual summer Landsat time series stacks (LTSSs). Both VCT and LandTrendr can reliably detect stand-clearing disturbance and regrowth patterns, but LandTrendr is better adapted to detecting partial disturbance and regrowth (Kennedy et al., 2010; Thomas et al., 2011). Abundant forest and forest disturbance commission errors have been problematic in some cases with VCT, particularly in complex and highly fragmented landscapes (e.g., Huang et al., 2010a; Walterman et al., 2008). To date, the largely successful validations of VCT and LandTrendr have mostly been restricted to a series of individual Landsat scenes scattered across the United States or, at most, multiple adjacent scenes encompassing an individual state. No wall-to-wall multistate, regional, or international assessments of these products exist.

1.1. Extensive forest commission errors in regional implementation of VCT

The North American Forest Dynamics (NAFD) project—funded by the National Aeronautics and Space Administration (NASA) and the USDA Forest Service—develops multitemporal change detection methods for archives of Landsat data with the goal of characterizing recent landscape trends in North American forest disturbance and regrowth. By extension, this work benefits the United States Environmental Protection Agency's (EPA) Great Lakes Restoration Initiative (GLRI) through the identification of spatial and temporal forest changes in the Great Lakes' drainage basins. In combination with field plot data collected by FIA, the resulting maps of forest changes facilitate the prioritization of landscapes for management and/or restoration activities. We chose the Lake Superior and Lake Michigan drainage basins (Fig. 1) as a starting point for applying VCT wall-to-wall across the Great Lakes in support of the GLRI. To accomplish this task, we downloaded 574 Landsat images for 36 paths/rows encompassing approximately 24.5 million ha (excluding Great Lakes waters) in the basins, acquired and/or generated necessary ancillary data for elevation and land cover, and applied VCT via procedures similar to those discussed by Huang et al. (2010a) and Thomas et al. (2011).

During preliminary quality assessments, we detected an abundance of false positives for forest and forest disturbance (i.e., commission errors). Visual inspections of aerial photography revealed that VCT erroneously included up to ~70% (locally) of nonforest pixels

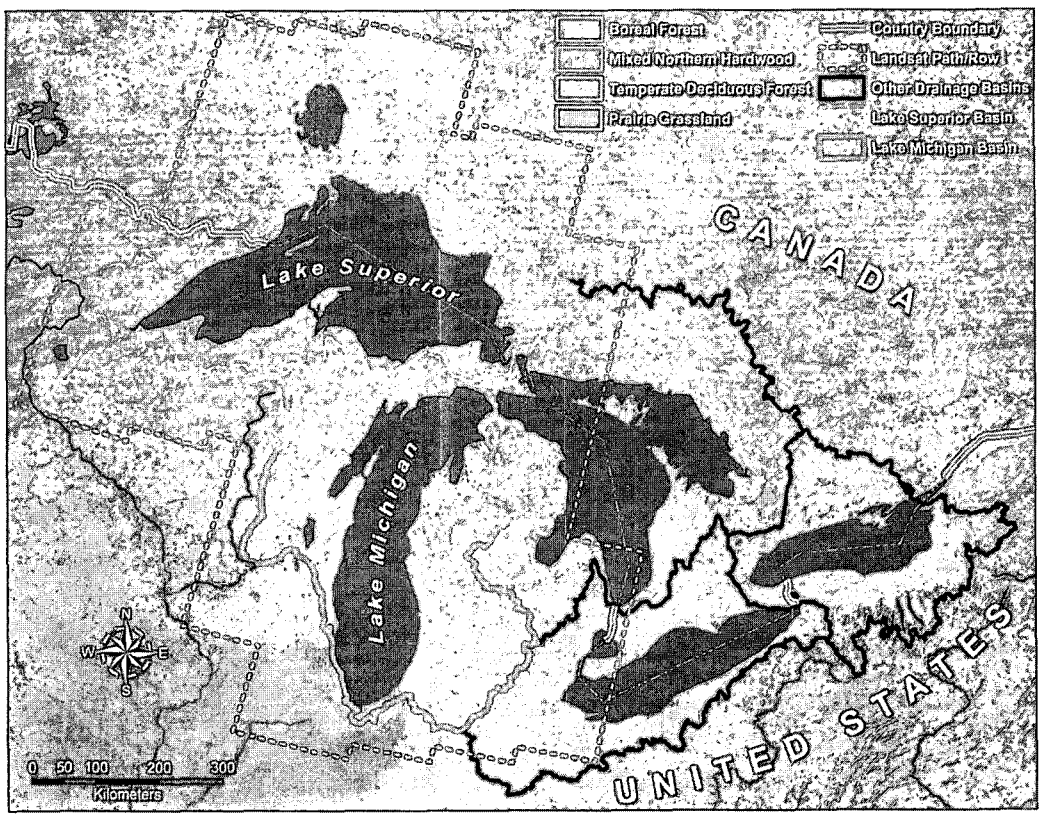

Fig. 1. The study area in the Great Lakes region of North America.
Data source: terrestrial ecoregions database from the World Wildlife Fund as presented by Olson et al. (2001).

in a disturbed forest or forest category. The preponderance of commission errors appeared to be associated with wetlands and agricultural fields in complex and highly fragmented forest landscapes (Fig. 2), consistent with reports from previous studies (Huang et al., 2010a; Thomas et al., 2011). These commission errors seemed logical because there is occasionally little spectral separability between forests, wetlands, and/or agricultural fields during the growing season (i.e., June through early September) (e.g., Odenweller & Johnson, 1984; Ozesmi & Bauer, 2002). Fluctuating water levels, highly variable vegetation densities across space and time, and differences in growing season phenology likely contribute to incorrect classifications in wetlands because these processes closely mimic spectral trajectories associated with healthy forest, disturbance, and regrowth (e.g., Ozesmi & Bauer, 2002) (upper panel of Fig. 3). A similar phenomenon likely occurs in agricultural landscapes (e.g., Odenweller & Johnson, 1984). Crops that senesce and are harvested early in the latter part of the growing season (especially wheat and soybeans) may simulate a forest disturbance and other years in the time series that include corn rotations, which usually do not senesce until the end of the growing season, likely exhibit a spectral resemblance to forest (upper panel of Fig. 3). Additionally, crops planted later in the growing season are sometimes mistaken as a disturbance because they have not emerged or have only recently emerged by the imagery acquisition date, whereas crops planted before the defined growing season fully emerged and are spectrally similar to forest.

1.2. Potential solutions

Forest commission errors have been reduced in national land cover classifications by utilizing imagery from multiple time periods per path/row, such as the early, peak, and late growing season Landsat imagery used to produce the National Land Cover Database (NLCD) (Homer et al., 2004). However, the VCT algorithm is mostly constrained to using imagery from the peak growing season and only incorporates later or earlier imagery during an abnormally warm fall or spring. Walterman et al. (2008) developed an effective solution to mitigate commission errors for forest and forest disturbance using random forests, 101 predictor variables, and 800 photo-interpreted points, but their approach is laborious and difficult to apply in regional landscapes (e.g., millions of hectares and larger) with widely varying reference data. We desired a convenient yet equally effective approach for comprehensive regional to international applications of VCT. Simply masking VCT outputs with nonforest classifications from other datasets, for example National Land Cover Data (NLCD) and other international equivalents, was not a viable option because these datasets comprise a temporally static representation of land cover and often suffer reduced accuracies in the same complex landscapes where VCT's performance declines (e.g., Wickham et al., 2004). Applying other algorithms to achieve a static forest/nonforest classification might also be useful, but this approach requires incorporating another classification technique and also does not capture the forest/nonforest boundaries continually shifting across time. However, acquiring multitemporal stacks of winter imagery may allow the exploitation of distinct spectral–thermal contrasts between forest and snow-covered nonforest landscapes to efficiently identify and mask nonforest areas over time.

Remote sensing scientists previously have utilized snow-covered winter imagery to improve maps of temperate and boreal forests, particularly when attempting to differentiate between deciduous and coniferous forest or to strictly map coniferous forest (Cohen et al., 2003; Wolter et al., 1995). In addition, snow-covered winter imagery may outperform growing season imagery when estimating forest structural attributes (e.g., basal area or volume) (Franco-Lopez et al., 2001). Distinct spectral–thermal separability occurs between snow-

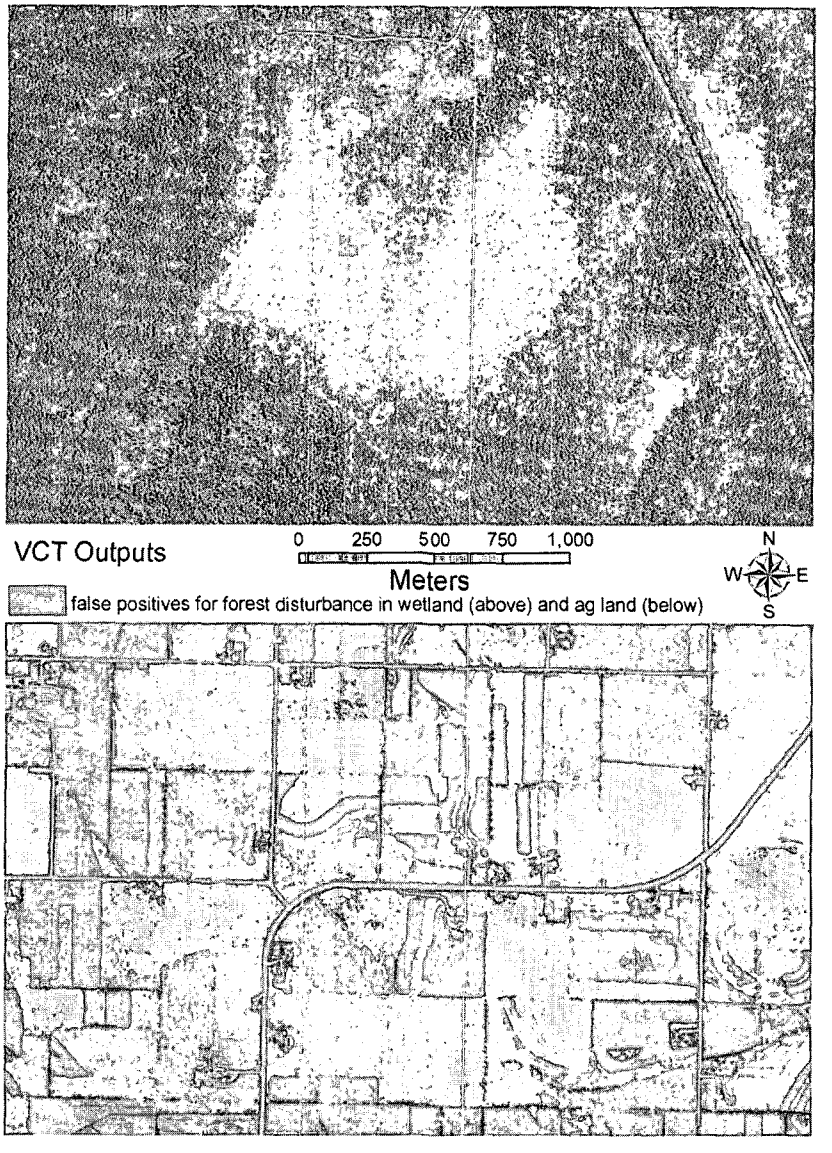

Fig. 2. Examples of the false positive errors for forest disturbance encountered during initial mapping procedures.

covered landscape features and forests. Snow reflects the majority of VNIR portions of the electromagnetic spectrum and much less in the SWIR portions, depending on viewing angle, snow consistency, and snow depth. Forests (especially coniferous) comparatively attenuate much of the reflectance, particularly in the visible portion of the electromagnetic spectrum but also in the near infrared bands, and reflect relatively more in the SWIR (cf. Warren, 1982; cf. Rock et al., 1986; Dozier, 1989; Vikhamar & Solberg, 2003a, 2003b; Vikhamar et al., 2004). In terms of thermal processes, bare and needled branches in forests absorb and convert more incoming shortwave radiation to longwave radiation compared to other snow-covered features on the landscape (Gustafsson et al., 2004; Sicart et al., 2004).

We postulated that applying VCT to snow-covered Landsat time series stacks (LTSSw) might generate an accurate nonforest mask capable of mitigating commission errors of forest and forest disturbance because the version of VCT utilized here includes an automated cloud-masking algorithm. This algorithm relies on the spectral–thermal Landsat bands to mask clouds from LTSSs (Huang et al., 2010b). Clear view forest pixels (i.e., uncontaminated by clouds or cloud shadows) are used to identify cloud boundaries and ultimately discern between clouds and clear view surfaces (Huang et al., 2010b). Pixel-based accuracies of this technique tested in data collected for the NAFD program range from 86.1% to 98.8%. This algorithm is likely to be equally proficient at masking snow-covered ground from LTSSw in relatively flat landscapes because of similar spectral–thermal contrast between both clouds/snow and other landscape features (Fig. 4) and improved spectral separation between forest and nonforest lands (lower panel versus the upper panel of Fig. 3) (Dozier, 1989). We proceeded with the key assumption that wetlands, agricultural fields, and other nonforest lands are largely frozen and covered with snow during a year with average to above average snowfall, and that the cloud-masking algorithm in VCT treats all of these snow-covered areas as "clouds", which subsequently can be integrated into the VCT processing stream as a nonforest mask.

Our primary objectives were to: (1) generate accurate maps of landscape changes from the mid-1980s to the present for the Lake Superior and Lake Michigan drainage basins of the western Great Lakes, (2) mitigate the prevalence of false positives for forest and forest disturbance persisting in VCT outputs, and (3) present a robust statistical assessment to gauge the effectiveness of incorporating snow-covered LTSSw in VCT. Achieving these objectives will represent a marked improvement in automated disturbance mapping protocols while generating more reliable spatially explicit maps of contemporary forest changes suitable for use in future research

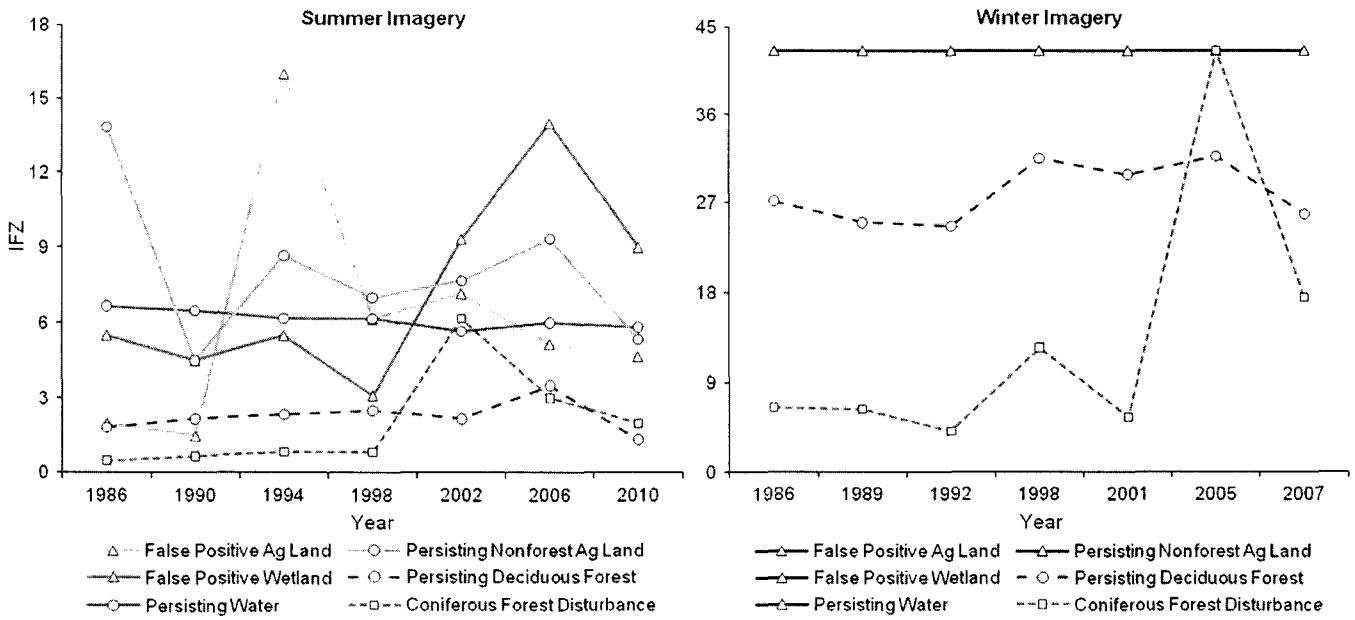

Fig. 3. Integrated forest z-scores (IFZ) for a random sample of pixel values extracted from stacks of summer (left panel) and snow-covered winter (right panel) imagery in p23r30 of southeastern Wisconsin. Calculating IFZ relies on Landsat TM or ETM+ bands 3, 5, and 7 (Huang et al., 2010a). We collected winter pixel values from the exact same locations as the sample of summer pixel values for each respective class. The summer scene demonstrates spectral confusion that can occur between forest and nonforest lands during the growing season. We truncated winter values at 42 to emphasize the greatly improved spectral separation between coniferous forest, deciduous forest, and other land cover types covered by snow during the winter. The only spectral overlap during winter occurred after the coniferous forest disturbance in the early 2000s, which is predictable and easily flagged for exclusion from a winter nonforest mask.

throughout the western Great Lakes region. It will also represent the first region-wide validation of VCT across a complex and spatially heterogeneous landscape that encompasses several dozen contiguous Landsat paths/rows.

2. Methods

2.1. Study area

This study was conducted within the Lake Superior and Lake Michigan basins of the western Great Lakes. These two lakes are located slightly east of the geographic center of North America and span across parts of both Canada and the United States, enclosed by a diverse landscape comprised of large tracts of contiguous and fragmented forest, wetlands, agricultural fields, lakes, human settlements, and frequent natural and anthropogenic disturbances. (Radeloff et al., 2005; Schulte et al., 2007; Stueve et al., 2011; Wolter et al., 2006) (Fig. 1). The spatial heterogeneity of this region is complex and landscape patterns often differ markedly over short geographic distances, dependent on physiographic features persisting from a glacial past, a phenological gradient affected by differences in temperature and precipitation, natural disturbances (especially wind, but also fire and insects), forest harvesting, agricultural activities, and a suite of development and preservation strategies. The landscape of the Lake Superior and Michigan drainage basins is particularly diverse and multifaceted because it also contains large tracts of boreal, mixed northern hardwood, and temperate deciduous forests (Fig. 1). The climate in the region is mostly humid continental with substantial influences on precipitation emanating from the Great Lakes (Bailey et al., 1994). According to the National Climatic Data Center (NCDC) and Environment Canada (EC), average annual temperatures in the region vary between 9.4 °C (southwest Michigan) and 0.3 °C (west half of northern Ontario), and average annual snowfall varies widely between 457 cm (western Upper Peninsula of Michigan) and 76 cm (southeastern Wisconsin). The heaviest annual snowfall amounts occur on the windward shores of the Great Lakes.

2.2. The VCT algorithm and constructing LTSSs

The VCT algorithm involves two major steps: (1) developing the LTSSs predicated on images ready for immediate use and (2) applying preprocessing, classification, and postprocessing algorithmic procedures (Fig. 5 flowchart displays where VCT fits in our broad processing scheme). Suitable LTSSs must include high quality Landsat Thematic Mapper (TM) and/or Enhanced Thematic Mapper Plus (ETM+) imagery, contain few or no clouds, stem from a defined peak growing season, achieve biennial or near-biennial frequency, and have proper geometric registrations and radiometric corrections (Huang et al., 2009). The United States Geological Survey (USGS) Global Visualization Viewer (GLOVIS) provides access to an extensive archive of Landsat imagery, most of which has been heavily processed to meet stringent specifications for level one terrain-corrected (L1T) data. VCT performs additional automated preprocessing of the Landsat imagery before masking clouded pixels, tracing the spectral responses of remaining pixels throughout the LTSSs, and commencing with the process of identifying persisting nonforest (PNF), persisting forest (PF), persisting water (PW), year of disturbance, damage severity (for natural disturbances, a combination of storm intensity and tree susceptibility), and rate of forest regrowth. Please see Huang et al. (2010a) for a more detailed description of all the necessary steps and relevant algorithms.

We acquired 574 summer Landsat images from GLOVIS (i.e., 5 TM and 7 ETM+) for 36 paths/rows encompassing the Lake Superior and Lake Michigan drainage basins at a near-biennial frequency. All imagery was L1T-processed, contained few or no clouds, and had a high (i.e., 9) quality rating. Undisturbed forests are relatively stable, spectrally, throughout much of the main growing season and allow the consideration of an array of imagery spanning several months. We broadly defined the growing season from early June to late September, but constrained collection of imagery to the peak growing season months of July and August whenever possible. We utilized imagery from earlier or later in the growing season only when cloud-free imagery was unavailable from the peak window for three consecutive years and in the presence of normal to above normal temperatures in the spring and fall, which reduced phenological deviations from peak season imagery.

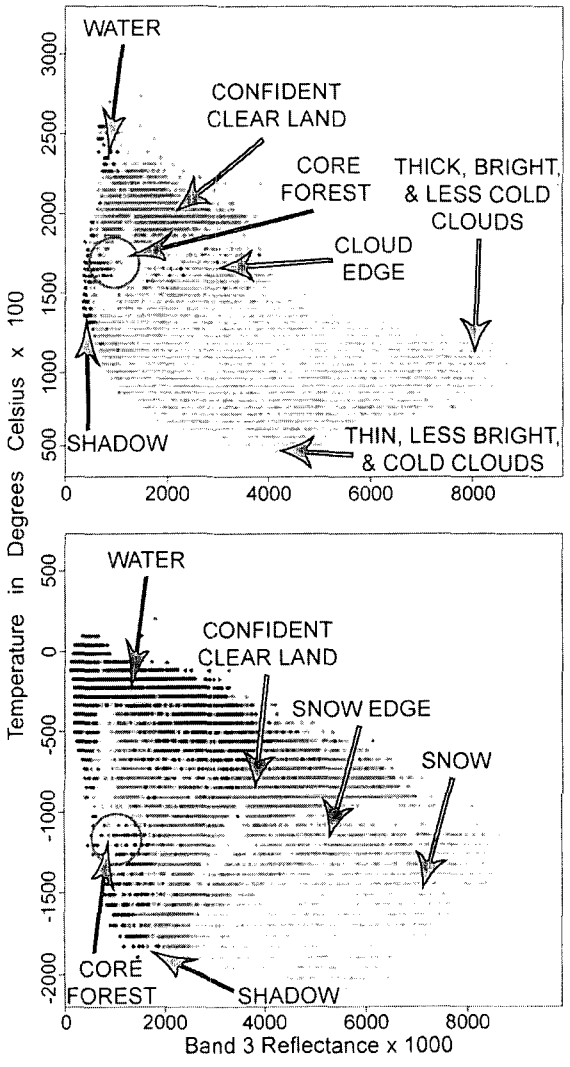

Fig. 4. Spectral-temperature space for a summer Landsat scene with clouds (upper panel) and a winter scene blanketed with snow containing no clouds (lower panel). Note the figures display identical patterns and that the snow has an even more distinct spectral–thermal space because it is consistently colder and highly reflective.

These criteria are consistent with established protocols for applying VCT (e.g., Huang et al., 2010a; Stueve et al., 2011; Thomas et al., 2011).

2.3. The VCT algorithm and constructing LTSSw

Understanding the selection criteria for imagery comprising the LTSSw necessitates an explicit and thorough description because there is no existing protocol for this specific application. We maintained some requirements analogous to the protocol for generating the LTSSs, such as utilizing high quality (i.e., preferably 9) Landsat TM or ETM+ imagery with few or no clouds and assuring images contained proper geometric registrations and radiometric corrections. Similar to the summer imagery, we acquired imagery for the LTSSw from GLOVIS that was L1T-processed. Likewise, VCT performed additional preprocessing to ensure the plying of sufficient corrections (e.g., Huang et al., 2010a; Thomas et al., 2011). In contrast to the summer protocol, every image used to create the LTSSw must contain comprehensive terrestrial snow cover because nonforest areas lacking snow are highly susceptible to erroneous exclusion from the nonforest mask (i.e., not interpreted as "cloud"). Therefore, we targeted the winter months of December–February during years with average to above average snowfall for our selections, occasionally venturing into March at northern latitudes and on windward shores of the Great Lakes. We avoided selecting imagery acquired less than one week after a major snowstorm in order to mitigate potential complications from decreased attenuation of spectral reflectance associated with tree limbs blanketed by fresh snow and spectral ambiguities associated with freshly fallen snow (i.e., compared to "old" snow) on exposed ground (e.g., Dozier, 1989; Vikhamar & Solberg, 2003b). We also tried to avoid selecting winter imagery after a major thaw event in order to circumvent exposed ground and the shifting spectral–thermal properties associated with melting snow (e.g., Vikhamar & Solberg, 2003b).

The first image in LTSSw must be absolutely cloud free and acquired from a date prior to the first image in LTSSs, which provides a reliable baseline to compare with subsequent imagery and avoids misclassifying forested pixels disturbed before the earliest image acquisition date in the LTSSs (i.e., likely in the midst of regrowth). The temporal density of LTSSw is lower in comparison to the summer imagery because largely cloud-free images with comprehensive snow cover are rare. Mostly cloud-free images were necessary because any persisting clouds could be erroneously included in the nonforest mask

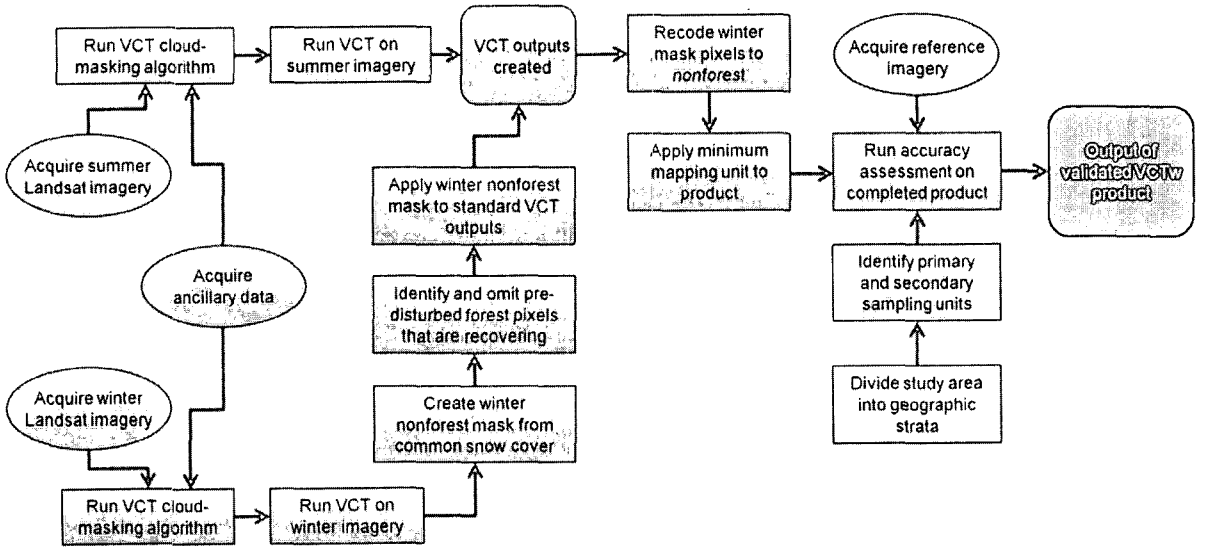

Fig. 5. Flowchart depicting the major steps involved in applying VCT to seasonal imagery, constructing a winter nonforest mask, validating classes in different strata, and generating the final VCTw product.

if they persisted in similar forested areas throughout the stack. This proved unproblematic because the objective of winter VCT applications is to identify nonforest areas presumably covered by snow and treated as "clouds", as opposed to correctly mapping forest disturbances. In most cases, we collected quadrennial imagery distributed as uniformly as possible across the LTSSw. Overall, we acquired 281 winter Landsat images from GLOVIS for 36 paths/rows in the Great Lakes region meeting the aforementioned criteria.

2.4. Acquiring and manipulating ancillary data

For successful implementation, VCT requires digital land cover, elevation, and Landsat data (Fig. 5) at similar spatial resolutions. We chose 30-m Landsat imagery as our baseline resolution. In the United States, the Multi-Resolution Land Characteristics Consortium (Homer et al., 2004, 2007) produced the 2001 NLCD at a 30-m resolution. A high quality digital elevation model (DEM) was accessible for both Canada and the United States from the USGS, derived from version 2 of the shuttle radar topography mission (SRTM). The 1-arc SRTM DEM available for the United States was already consistent with the 30-m Landsat data. In Canada, 1-arc SRTM DEMs are not available. We therefore oversampled the 3-arc SRTM to 30-m in order to expeditiously generate a suitable DEM encompassing our area of interest. We deemed this solution sufficient for the relatively flat landscape of the Lake Superior basin in southern Canada (Ontario), which has much less topographic variability relative to mountainous regions and is ultimately less likely to influence VCT image preprocessing algorithms.

The NLCD is not available in Canada. However, the Earth Observation for Sustainable Development of Forests, a joint project between the Canadian Forest Service and Canadian Space Agency, provided a land cover map of all forested areas in Canada. This land cover map encompasses large portions of southern Canada and overlaps with the Great Lakes drainage basins at a spatial resolution comparable to the NLCD and Landsat data. We recoded forest and nonforest pixels from the Canadian land cover map to values matching similarly classified pixels from the NLCD. VCT simply utilizes land cover data to automatically extract samples of pixels from probable forest areas and evaluates their spectral signatures. Therefore, discrepancies between the land cover mapping protocols for Canada and the United States are unlikely to exert a substantial influence on VCT output products.

2.5. Running VCT and creating the winter nonforest mask

Executing VCT for the summer imagery (Fig. 5) produced standard outputs denoting PNF, PF, PW, year of disturbance, damage severity, and rate of forest regrowth (top row of Fig. 6, examples of PNF, PF, and disturbance). For the winter, selectively applied preprocessing and cloud mapping algorithms embedded in VCT generated individual image outputs denoting "clouds" for all areas sufficiently covered in snow (i.e., the raw nonforest mask for each year) (middle and bottom rows of Fig. 6). This intentional misapplication of VCT's cloud masking algorithm with LTSSw ultimately resulted in the mapping of snow across exposed areas lacking trees, which we subsequently recoded as nonforest for use in a post-processing mask of summer VCT outputs. Additional steps necessary for refining the winter nonforest mask include augmenting VCT with various algorithmic components in a processing model.

The first part of the processing model identifies the common spatial extent of all pixels covered by snow throughout the entire stack, as determined by the cloud mapping algorithm (middle and bottom rows of Fig. 6). The second part identifies and omits pixels likely disturbed prior to the year of the first winter image in each stack. This is a crucial step in some areas because a slow post-disturbance forest recovery may erroneously appear as snow-covered nonforest throughout much of the winter stack, producing commission errors in the winter nonforest mask that would ultimately contribute to forest disturbance errors of omission. The sum of differences between integrated forest z-score (IFZ) (Huang et al., 2010a) values from the first summer image and subsequent images in the summer stack facilitated the identification of pixels suitable for omission, calculated as follows:

$$\sum_{i=2}^{NY} (IFZ_1 - IFZ_i) \quad (1)$$

where *NY* is the number of years in the LTSSs and *IFZ* is the integrated forest z-score for any pixel from the designated year. IFZ measures the distance of a pixel to the center of forest pixels in the spectral domain, which is normalized by the standard deviation of forest pixels. Integrated values from Landsat TM and ETM+ bands 3, 5, and 7 are used to calculate IFZ because bands 1 and 2 are correlated with band 3, and band 4 (near infrared) sometimes provides inconsistent spectral responses in forested landscapes (Huang et al., 2010a). Low IFZ scores (i.e., <3) are indicative of forest. Consequently, comparatively low sum of differences values likely represent areas of concern in wetlands and fields, whereas relatively large values likely identify areas of slowly recovering forest suitable for exclusion from the nonforest mask. Visual observations and interpretations suggested a threshold value of 0.4 was appropriate for the sum of differences between IFZ values. Applying the winter nonforest mask to the standard VCT forest disturbance output produced an appropriately refined product (bottom row of Fig. 6), where any forested or disturbed pixels falling within the boundaries of the mask are recoded to nonforest. Lastly, a minimum mapping unit (MMU) of 4 pixels (0.36 ha) was applied, similar to one of the procedures used by Thomas et al. (2011) for postprocessing of standard VCT products. We dubbed this combined process VCTw.

2.6. Assessment procedures

The accuracies of PNF, PF, PW, disturbed 1985–1999 (D1), and disturbed 2000–2008 (D2) were assessed for both VCT and VCTw. Year of disturbance was binned into two groups because the cost and insufficient coverage of the validation data disallowed a comprehensive accuracy assessment at finer temporal resolutions. In order to estimate the accuracies of the VCT and VCTw products, we mosaiced all paths/rows and selected a two-stage cluster sample, relying on insight from techniques discussed by Nusser and Klaas (2003) and Stehman et al. (2003). To initiate this task, we partitioned our entire study area into four geographic strata based on land use, seasonality, development, and international borders (Fig. 7). Lower Lake Michigan basin (LLMB) has sparse forest cover (mostly deciduous), abundant agricultural land, and substantial development at the lowest latitude; upper Lake Michigan basin (ULMB) has abundant forest (deciduous/coniferous mix), some agricultural land, and some development at a relatively low latitude; lower Lake Superior basin (LLSB) has abundant forest (more coniferous, less deciduous) and some development at a relatively high latitude; and upper Lake Superior basin (ULSB) has abundant forest (mostly coniferous), widespread disturbances, and some development at the highest latitude. LLMB, ULMB, and LLSB are fully confined within the USA; ULSB is fully confined within Canada. Some of these factors may interact at the regional scale to create distinct patterns of variability in accuracy across space (e.g., Foody, 2002), which suggested it was prudent to draw independent samples from each geographic stratum with designs tailored to their individual characteristics. Financial and technical constraints prevented us from assessing the ULSB with this design. For the three USA strata, we used two-stage cluster sampling to reduce the number of aerial photographs necessary for preparation. Primary sampling units (PSUs) were constructed from the boundary tiles of aerial photography archives (~13,500 ha each) (Fig. 7). There

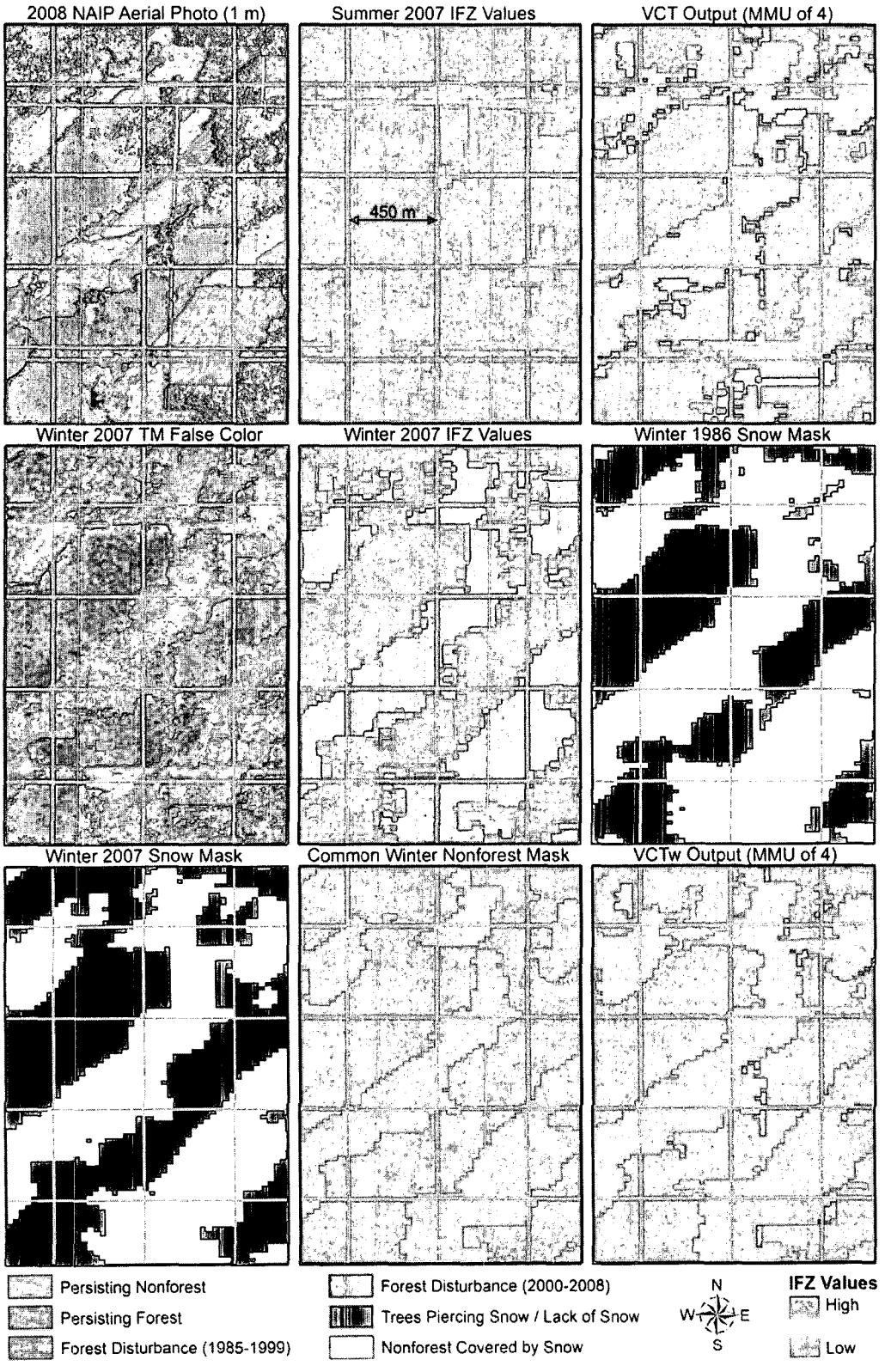

Fig. 6. A schematic flow (by row) for procedures involved in enhancing the VCT output product and generating VCTw, beginning with the left panel in the top row. Calculating IFZ values relies on Landsat TM or ETM+ bands 3, 5, and 7 (Huang et al., 2010a). Notice the difference in spectral contrast between forest/nonforest in the summer and winter.

were 269 PSUs in LLMB, 347 in ULMB, and 173 in LLSB respectively. A simple random sample based on the approximate area of each geographic stratum was applied to select a corresponding subset of PSUs, including 35 in both LLMB and ULMB, and 17 in the LLSB (Fig. 7). In each PSU, we employed a secondary stratified random sample of all pixels to facilitate the selection of secondary sampling units (SSUs) representing the five defined classes of output products (Table 1). In each PSU, we assessed a total of 40 (LLSB), 24 (ULMB), or 32 SSUs (LLMB) respectively. The number of SSUs or pixels corresponding to each class varied from two to ten, depending on the class type and basin

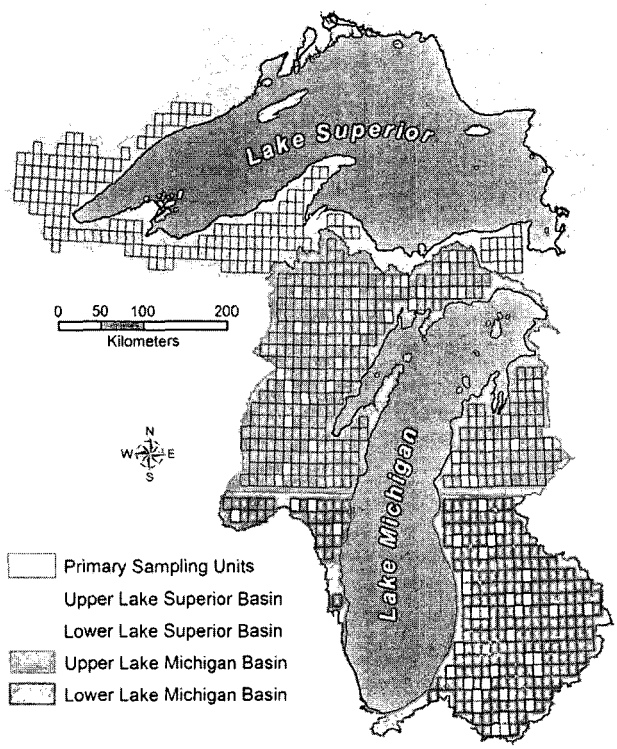

Fig. 7. Geographic strata utilized in the sampling procedures for the accuracy assessments.

it occupied (Table 1). Predicated on this sample, we used ratio estimation to generate a confusion matrix, user's accuracies, and producer's accuracies for both VCT and VCTw. Linearized variances were used to estimate standard errors for all ratio estimators (Särndal et al., 1992).

In terms of interpreting whether pixels were correctly classified in the SSUs, we first visually compared the placement of pixels in the PSUs with National Agricultural Imagery Program (NAIP) archives in a geographic information system (GIS) environment. NAIP was used as a baseline because it provides optimum spatial resolution (1 m) for determining general class types (i.e., forest, nonforest, and water) across large geographic extents. Subsequently, NAIP imagery was visually compared with National Aerial Photography Program (NAPP) and National High Altitude Program (NHAP) archives to detect any potential discrepancies or change. The texture and shape of areas of interest in the NAPP and NHAP imagery were most helpful for detecting changes because their spatial resolutions are relatively coarse (i.e., ~2 m). In the rare cases where this procedure generated any uncertainty, multispectral Landsat imagery was used for additional interpretations. Winter Landsat imagery proved most useful in detecting forest disturbances that recovered quickly or occurred between distant gaps in the aerial reference imagery. Although the spatial resolution of the Landsat imagery (i.e., 30 m multispectral) is coarser than the aerial photography, it was invaluable because of superior temporal and spectral resolutions. The exploitation of the Landsat archive was strictly limited to cases with ambiguous outcomes after interpreting the aerial photography or when there was a large gap in the aerial photography archives.

Table 1
The number of SSUs selected from each map class during the second sampling phase. PF = persisting forest, PNF = persisting nonforest, PW = persisting water, D1 = disturbed early (1985–1999), and D2 = disturbed late (2000–2008). Region codes are LLSB = lower Lake Superior basin, ULMB = upper Lake Michigan basin, and LLMB = lower Lake Michigan basin.

	PNF	PF	PW	D1	D2
LLSB	9	9	2	10	10
ULMB	5	5	2	6	6
LLMB	7	7	2	8	8

We conducted comparisons between VCT and VCTw outputs by computing pairwise difference scores according to the correctness of the classifications made for each pixel sampled. Specifically:

$$d_k = \begin{cases} +1 & \text{if VCTw correct, VCT incorrect} \\ 0 & \text{if both correct or both incorect} \\ -1 & \text{if VCTw incorrect, VCT correct} \end{cases} \quad (2)$$

was computed for the k^{th} pixel in the sample. Ratio estimators and linearized estimated standard errors were used to estimate the mean difference in accuracy between VCT and VCTw products, and 95% normal-based confidence intervals were computed around these estimators. Note that the true coverage probability of normal-based confidence intervals is unknown in such a complex sampling design.

All computations in this section were executed using the statistical software *R* 2.10.0 and the package "survey" (Lumley, 2004, 2010; R Development Core Team, 2010). Additional details about this section are forthcoming (Zimmerman et al., in progress).

In addition to the site-specific procedures described above, we conducted non-site specific comparisons of aerial extent of forest and nonforest classes. Map-based counts of pixels were tabulated to produce area estimates from VCT- and VCTw-based map categories for the entire study area, Lake Superior basin, Lake Michigan basin, LLSB, ULMB, and LLMB. No estimates of uncertainty were available for map-based estimates of area. Estimates and sampling errors of forest and nonforest for LLSB, ULMB, and LLMB also were produced from strategic forest inventory data obtained from the USDA Forest Service FIA program. A comparison of VCTw- and FIA-based area estimates was conservatively reported as being statistically significantly different if a map-based estimate fell outside the bounds of an approximate 95% confidence interval surrounding an FIA-based estimate.

3. Results

3.1. VCT

According to output products from VCT, there was approximately 5.368 million ha of PNF, 15.407 million ha of PF, 1.278 million ha of PW, 1.360 million ha of D1, and 1.010 million ha of D2 combined in the entire study area throughout the Lake Superior and Lake Michigan drainage basins (Figs. 8 and 9). The overall accuracy was 86.3% (Fig. 10, Table 2) and the standard error was 1.2%. The standard error for each class was 2.0% or less (Table 3). Commission errors (100%−% user's accuracy) ranged from 54.4% (D2) to 0.3% (PW) and omission errors (100%−% producer's accuracy) varied from 52.9% (D1) to 4.3% (PF) (Table 4). The omission error for PNF was about four times greater than the commission error and, conversely, the commission error for PF was about three times greater than the omission error. Errors of commission and omission were relatively consistent for PW, D1, and D2. The standard error for user's and producer's accuracies remained low (<2.5%) for the majority of classes (PNF, PF, and PW), but increased above 5% for D1 and D2 (Table 4).

When considering each of three geographic strata for VCT, the proportion of total area for PNF increased rapidly from the LLSB to the

LLMB, while PF decreased rapidly from the LLSB to the LLMB. PW was highest in the ULMB and lowest in the LLMB, and disturbed forest (D1 and D2) was slightly lower in the LLMB and identical in the remaining two basins (Figs. 8 and 9). The overall accuracy was lowest in the LLSB (82.9%) and highest in the LLMB (88.0%) (Fig. 10, Table 5) while the standard error never exceeded 3%. The standard error for each class of individual strata never surpassed 4% (Table 6). Commission errors ranged from 82.3% (D2 of the LLMB) to 0.0% (PW of the LLSB) and omission errors varied from 62.1% (D2 of the LLSB) to 0.5% (PF of the LLSB). Once again, the omission error for PNF greatly exceeded the commission error and, likewise, the commission error for PF was greater than the omission error (Table 7). The commission and omission errors for PW were fairly consistent, except for some differences in the LLSB and the LLMB. However, large discrepancies surfaced in D1 and D2. In the LLSB and the ULMB, the commission errors for disturbance were much lower than the omission errors (Table 7). In the LLMB, conversely, the commission error for disturbance greatly exceeded the omission error.

3.2. VCTw

VCTw denoted approximately 6.466 million ha of PNF, 14.663 million ha of PF, 1.268 million ha of PW, 1.146 million ha of D1, and 0.853 million ha of D2 (Figs. 8 and 9). The overall accuracy was 91.2% (Fig. 10, Table 2) and the standard error was 0.8%. The standard error for each class was 2.1% or less (Table 3). Commission errors ranged from 25.0% (D2) to 0.3% (PW) and omission errors varied from 53.5% (D2) to 4.3% (PW) (Table 4). Errors of commission and omission for PNF, PF, and PW exhibited identical values below 10%. Commission errors were generally much lower than omission errors for both D1 and D2. The standard error for user's and producer's accuracies remained relatively low (<3.5%) for most classes (PNF, PF, and PW) and the user's accuracies of D1 and D2, but increased above 5% for the producer's accuracies of D1 and D2 (Table 4).

When considering each of three geographic strata for VCTw, the proportion of total area for PNF increased rapidly from the LLSB to the LLMB, PF decreased rapidly from the LLSB to the LLMB, PW was highest in the ULMB and lowest in the LLMB, and disturbed forest (D1 and D2) decreased steadily from the LLSB to the LLMB (Figs. 8 and 9). The overall accuracy was lowest in the LLSB (87.0%) and highest in the LLMB (94.6%) (Fig. 10, Table 5) while the standard error never exceeded 2.2%. The standard error for each class of individual strata never exceeded 3.8% (Table 6). Commission errors ranged from 59.7% (D2 of the LLMB) to 0.0% (PW of the LLSB) and omission errors ranged from 63.8% (D2 of the LLSB) to 1.1% (PF of the LLSB). Once again, the commission and omission errors for PNF, PF, and PW were identical, except for the LLSB (Table 7). Commission errors for D1 and D2 were

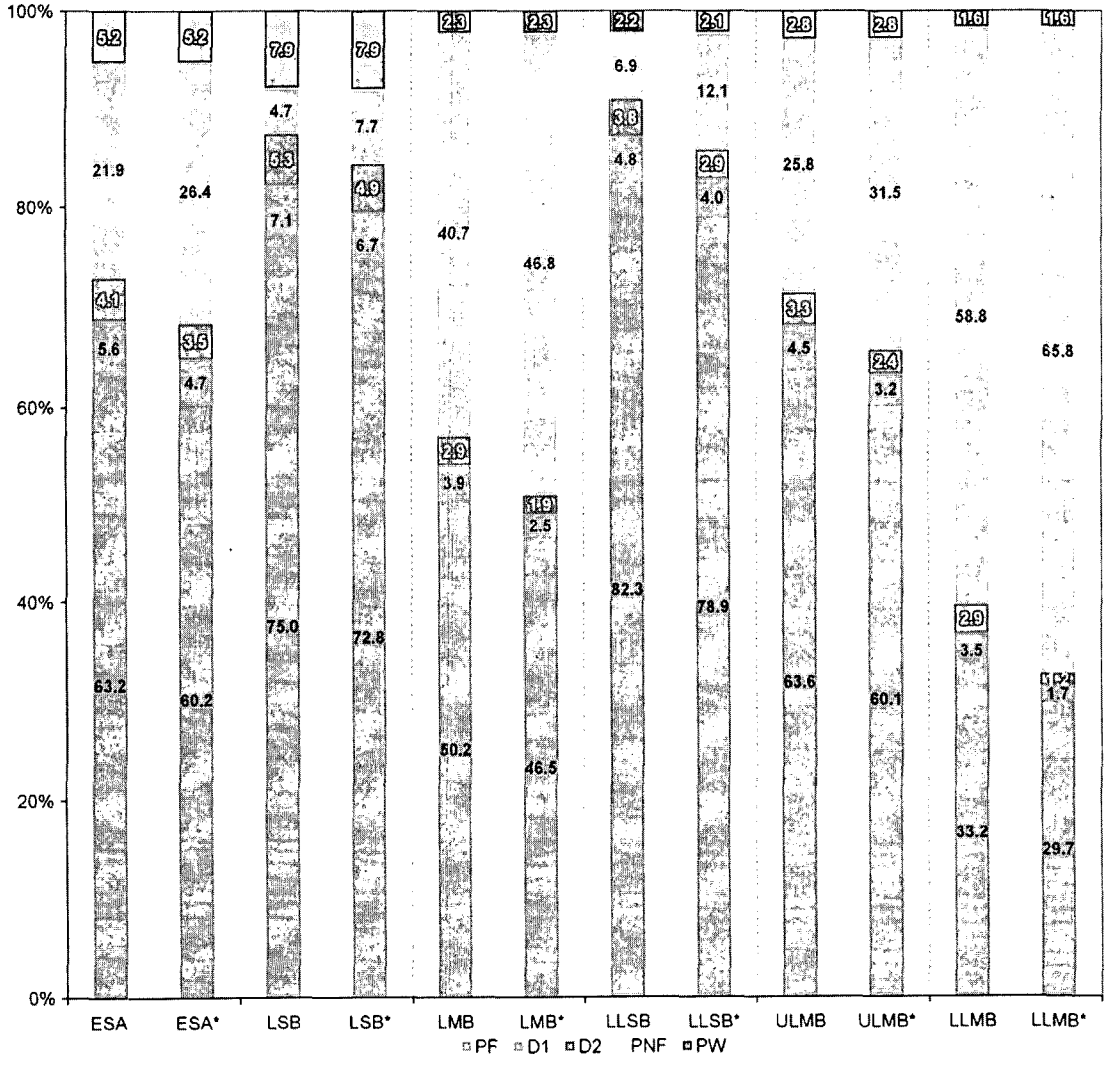

Fig. 8. Comparisons of percent cover for all five classes throughout the entire study area (ESA, 24.378 million ha), Lake Superior basin (LSB, 12.718 million ha), Lake Michigan basin (LMB, 11.659 million ha), lower Lake Superior basin (LLSB, 4.378 million ha), upper Lake Michigan basin (ULMB, 6.475 million ha), and lower Lake Michigan basin (LLMB, 5.184 million ha) for both VCT (no asterisk) and VCTw (with asterisk).

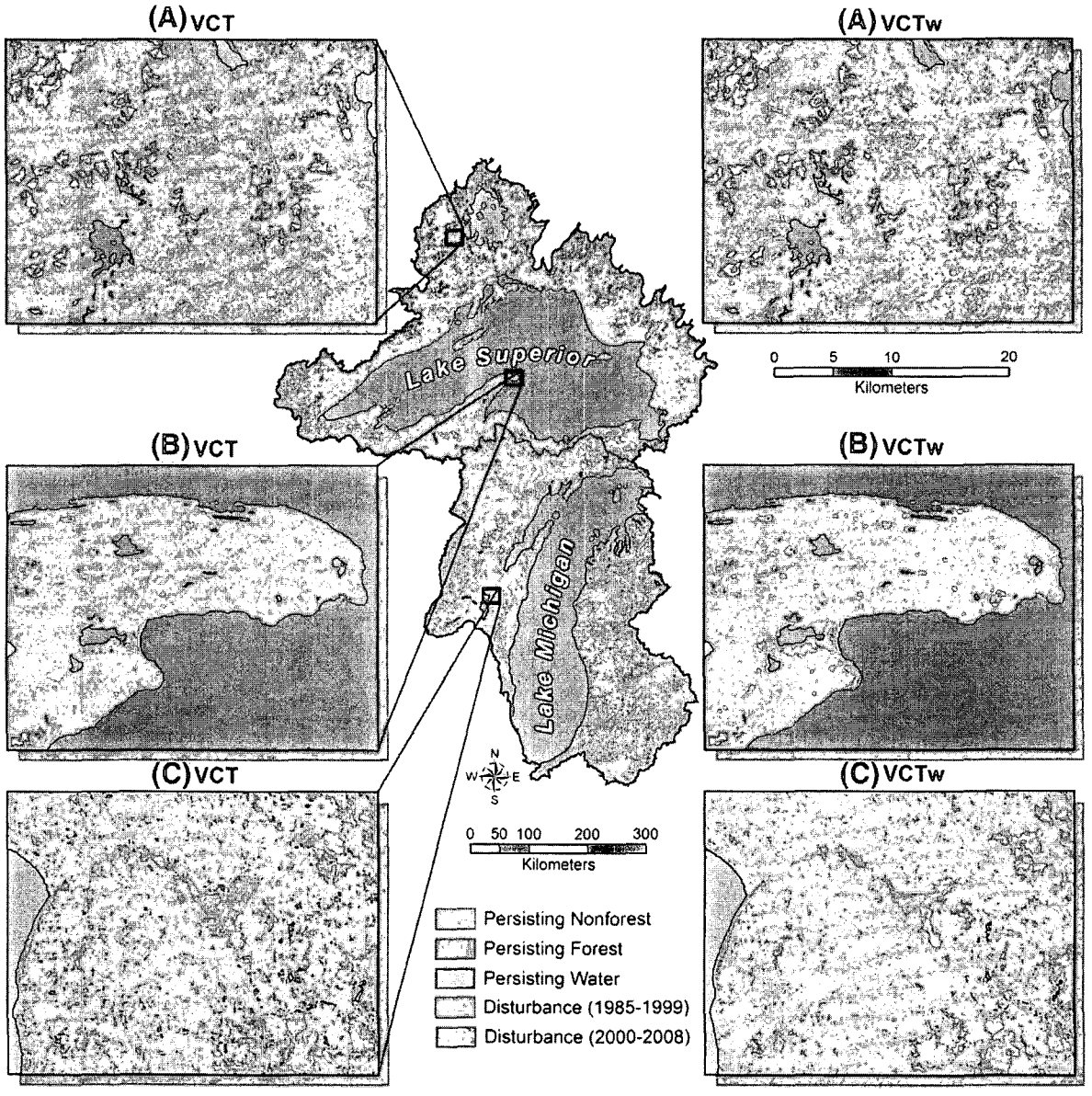

Fig. 9. Overview map based on VCTw and subset maps based on both VCT and VCTw.

less than the omission errors in the LLSB and the ULMB, but were somewhat identical in the LLMB (Table 7).

3.3. VCT versus VCTw

Compared to VCT, VCTw denoted more PNF (1.098 million ha), less PF (−0.744 million ha), similar PW, less D1 (−0.214 million ha), and less D2 (−0.157 million ha) throughout the entire study area. The difference between the overall accuracies of VCTw and VCT was estimated to be nearly 5% with a narrow standard error of 0.89 (Table 8). An analogous trend of improvement materialized in the different geographic strata, although VCTw effected the most improvement in the LLMB (+6.62%) and the least, yet statistically significant improvements (as assessed by a Normal-based 95% confidence interval), in the LLSB and ULMB (+4.09% and +3.84% respectively) (Table 8). Most classes performed similar to the entire study area, except for an anomaly in the LLMB where the area of disturbed forest (both D1 and D2) denoted by VCT was nearly two times higher than denoted by VCTw.

3.4. Forest area estimates

FIA estimates of forest land displayed no statistically significant difference when comparing the early (1985–1999) and late (2000–2008) periods for any of the three US strata (LLSB, ULMB, and LLMB). Therefore, subsequent results are confined to comparisons within the late period. VCT estimates were statistically significantly higher than FIA estimates for all three US strata during the late period (Fig. 11). Compared to VCT, VCTw estimates of forest land area were 5.0, 6.6, and 14.3% lower for LLSB, ULMB, and LLMB, respectively (Fig. 11). VCTw estimates exhibited no statistically significant difference from FIA estimates in the LLSB and ULMB, but the VCTw estimate was significantly higher for LLMB (Fig. 11).

4. Discussion

This study successfully implemented and validated regional wall-to-wall applications of VCT and VCTw across a complex and spatially heterogeneous forest landscape in the Lake Superior and Lake Michigan

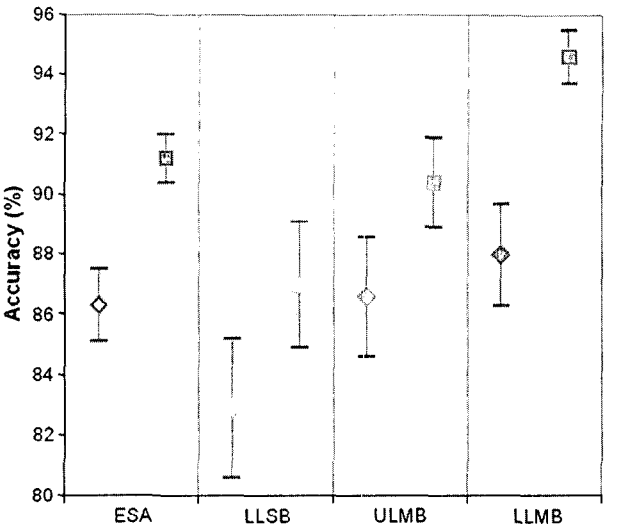

Fig. 10. Overall accuracies for VCT (diamonds) and VCTw (squares) with 95% confidence interval bars.

drainage basins of the western Great Lakes. The superior overall performance of VCTw was likely a positive consequence of significant spectral–thermal contrast between forest and nonforest lands on snow-covered winter Landsat imagery (Figs. 3 and 4). Even the leafless deciduous forest attenuated enough of the snow's reflectance to avoid confusion with other snow-covered features (Fig. 3), making the assumption of a transparent leafless deciduous forest canopy dubious (e.g., Vikhamar & Solberg, 2003a). Although, the dissipation of heat from bare tree limbs and needles absorbing incoming shortwave radiation also was likely a major contributor to enhancing forest–nonforest thermal differences during the winter months and creating a reliable nonforest mask (Gustafsson et al., 2004; Sicart et al., 2004). The strengths of this basic binary spectral–thermal relationship between forest and completely snow-covered nonforest in remote sensing applications are well established, a consequence of snow reflectance being partially occluded from the sensor by the forest canopy, the different physical properties of snow under forest canopies influencing spectral reflectance, and the comparatively cooler temperature of snow in exposed snow-covered areas (Sicart et al., 2004; Vikhamar et al., 2004; Vikhamar & Solberg, 2003b; Warren, 1982). Exploiting the sharp spectral–thermal contrasts between land cover types during the winter season ultimately enabled the efficient mitigation of false positives for forest and forest disturbance associated with wetlands and agricultural lands. Marked decreases in the percent commission errors (i.e., 100%—user's accuracy percent) for PF, D1, and D2, and a simultaneous larger decrease in the percent omission error (i.e., 100%—producer's accuracy percent) for PNF indicate that many false positives for forest and forest disturbance were removed by the nonforest mask and appropriately coded to nonforest. Consistently low commission errors for PNF (~6%), omission errors for PF (~5%), and commission (~0%) and omission (~5%) errors for PW when either VCT or VCTw were applied indicate that VCTw continued to effectively classify these classes while improving the others.

The influence of landscape variability on accuracy assessments across a complex latitudinal landscape gradient is immediately apparent when observing the accuracy assessments of the three geographic strata. The remote sensing community recognizes the potential for spatial variability of accuracy, but seldom provides more robust accuracy assessment strategies to address the problem (Foody, 2002). Dividing large geographic extents into different geographic strata within an intuitive landscape ecological framework, as employed in this paper, appears to be a justifiable and useful approach because disparate land cover and land use types may influence spectral reflectance, thermal emissivity, and ultimately accuracy (Zimmerman et al., in progress; Duguay, 1995; Sicart et al., 2004).

The comparatively high overall accuracy of VCTw in the LLMB was initially perplexing because it appeared counterintuitive to obtain optimum VCTw performance in a highly fragmented and sparsely forested landscape with few large areas of contiguous forest, especially when considering that this was the only stratum where VCTw estimates did not precisely correspond with FIA estimates of forest land area. One plausible explanation of this observation involves the high proportion of deciduous trees that dominate the landscape in the LLMB. Deciduous trees shed their leaves every fall and exposed limbs and branches are subsequently much less likely to

Table 2
Confusion matrix estimates for VCT (not shaded) and VCTw (shaded) representing the entire study area. Columns represent the respective VCT or VCTw class and rows represent the validation class.

	PNF	PF	PW	D1	D2
PNF	29.6	5.4	0.0	1.0	1.2
	34.9	1.8	0.0	0.2	0.3
PF	1.3	51.2	0.0	0.6	0.4
	2.1	50.9	0.0	0.4	0.2
PW	0.1	0.0	1.7	0.0	0.0
	0.1	0.0	1.7	0.0	0.0
D1	0.2	1.9	0.0	2.4	0.0
	0.3	1.9	0.0	2.3	0.0
D2	0.0	1.5	0.0	0.0	1.4
	0.0	1.5	0.0	0.0	1.4

Table 3
Confusion matrix standard error (SE) estimates for VCT (not shaded) and VCTw (shaded) representing the entire study area.

	PNF	PF	PW	D1	D2
PNF	1.9	0.8	0.0	0.2	0.3
	2.1	0.5	0.0	0.0	0.0
PF	0.3	2.0	0.0	0.2	0.2
	0.4	2.0	0.0	0.1	0.0
PW	0.0	0.0	0.3	0.0	0.0
	0.0	0.0	0.3	0.0	0.0
D1	0.1	0.5	0.0	0.4	0.0
	0.2	0.5	0.0	0.3	0.0
D2	0.0	0.5	0.0	0.0	0.2
	0.0	0.5	0.0	0.0	0.2

Table 4
User's and producer's accuracy estimates for VCT (not shaded) and VCTw (shaded) representing the entire study area.

	User's accuracy		Producer's accuracy	
	Estimate	SE	Estimate	SE
PNF	94.8	1.1	79.5	2.2
	93.2	1.1	93.8	1.3
PF	85.3	1.7	95.7	0.7
	90.7	1.3	95.0	0.8
PW	99.7	0.2	94.7	2.2
	99.7	0.2	95.7	1.7
D1	59.4	5.2	53.2	7.5
	79.3	3.3	51.1	7.3
D2	45.6	6.4	47.1	7.6
	75.0	2.8	46.5	7.5

intercept snowfall throughout the winter (Suzuki et al., 2008; Vikhamar & Solberg, 2003b). Additionally, if snow accumulates on a deciduous tree, their structural branch pattern prevents large quantities of snow from collecting in a common area that could dramatically increase reflectance (Suzuki et al., 2003, 2008; Vikhamar & Solberg, 2003b). Conversely, the propensity for evergreen conifer trees to intercept snowfall is higher because their needles persist throughout the winter, and snowfall is more apt to accumulate in a common conical area that may greatly increase reflectance (Suzuki et al., 2008; Vikhamar & Solberg, 2003b). Therefore, increased snowfall interception in the canopies of the relatively abundant coniferous forest in the ULMB and LLSB may have slightly tempered the overall accuracy of VCTw because of potential spectral confusion with snow-covered nonforest lands. This phenomenon was likely exacerbated where stunted coniferous trees intermix with exposed bedrock that has been heavily scoured by glaciers, blurring the forest–nonforest boundary (less common in the LLMB). A slight increase in the commission error for PNF and corresponding decrease in the omission error for PF in both the LLSB and ULMB lend credence to this claim. Thermal differences between snow-covered deciduous and coniferous trees likely did not enhance this spectral effect because corresponding radiation balances are identical (Suzuki et al., 2003). A second possible contributing factor is that VCTw performed better on agricultural lands as opposed to wetlands. Agriculture is comparatively abundant in the LLMB whereas wetlands especially dominate many nonforest landscapes in the LLSB. Wetland vegetation, unlike most agricultural lands, may regularly protrude from an otherwise comprehensive snow cover (e.g., Ozesmi & Bauer, 2002). Relatively high omission errors for PNF and high commission errors for PF, D1, and D2 in the mostly coniferous forest of the LLSB support this claim. It is probable that a combination of the aforementioned factors slightly suppressed the overall accuracy of VCTw in the ULMB and LLSB, but the evidence presented here is purely circumstantial. Regardless, VCTw continually outperformed VCT in every geographic stratum.

VCTw did not improve the omission errors for D1 and D2 and, in some cases (i.e., LLMB) VCTw only decreased the commission errors for D1 and D2 to a still unsatisfactory 50–60%. When considering most of the other classes exhibited commission or omission errors of 10% or much less in each geographic stratum and throughout the entire study area, these observations suggest VCTw had difficulty detecting forest disturbances and/or that there was some confusion between manual interpretations of validation data and VCTw disturbance classes. Partial forest disturbances are especially problematic in terms of aligning visual interpretations of aerial photography or satellite imagery with a VCT disturbance class (Huang et al., 2010a). This is a known hindrance when validating data, especially when precluding the use of ground reference points and exclusively relying on remotely sensed imagery (Foody, 2002). To complicate matters

Table 5
Confusion matrix estimates for VCT (not shaded) and VCTw (shaded) representing the lower Lake Superior basin[1], upper Lake Michigan basin[2], and lower Lake Michigan basin[3]. Columns represent the respective VCT or VCTw class and rows represent the validation class.

	PNF	PF	PW	D1	D2
PNF[1]	6.4	6.4	0.0	0.7	1.7
	11.0	3.9	0.0	0.1	0.2
PF[1]	0.1	68.2	0.0	0.2	0.0
	0.5	67.8	0.0	0.1	0.0
PW[1]	0.1	0.1	2.2	0.0	0.0
	0.1	0.0	2.3	0.0	0.0
D1[1]	0.1	4.5	0.0	4.1	0.0
	0.2	4.4	0.0	4.0	0.0
D2[1]	0.0	3.2	0.0	0.0	2.0
	0.1	3.2	0.0	0.0	1.9
PNF[2]	19.1	5.3	0.0	0.6	0.5
	23.5	1.6	0.0	0.1	0.2
PF[2]	1.4	61.4	0.0	0.8	0.7
	2.9	60.8	0.0	0.4	0.2
PW[2]	0.0	0.0	1.5	0.0	0.0
	0.0	0.0	1.5	0.0	0.0
D1[2]	0.3	1.9	0.0	2.8	0.0
	0.3	1.9	0.0	2.8	0.0
D2[2]	0.0	1.9	0.0	0.0	1.9
	0.0	1.9	0.0	0.0	1.9
PNF[3]	56.1	4.9	0.0	1.7	1.9
	62.9	0.9	0.0	0.3	0.4
PF[3]	1.9	28.8	0.0	0.7	0.2
	2.1	28.8	0.0	0.5	0.2
PW[3]	0.1	0.0	1.7	0.0	0.0
	0.1	0.0	1.7	0.0	0.0
D1[3]	0.3	0.2	0.0	0.9	0.0
	0.6	0.2	0.0	0.7	0.0
D2[3]	0.0	0.1	0.0	0.0	0.5
	0.0	0.1	0.0	0.0	0.5

Table 6
Confusion matrix standard error (SE) estimates for VCT (not shaded) and VCTw (shaded) representing the lower Lake Superior basin[1], upper Lake Michigan basin[2], and lower Lake Michigan basin[3].

	PNF	PF	PW	D1	D2
PNF[1]	1.9	1.4	0.0	0.3	0.8
	2.6	1.4	0.0	0.1	0.0
PF[1]	0.1	2.7	0.0	0.1	0.0
	0.2	2.6	0.0	0.1	0.0
PW[1]	0.1	0.0	1.1	0.0	0.0
	0.1	0.0	1.1	0.0	0.0
D1[1]	0.1	1.8	0.0	1.4	0.0
	0.1	1.8	0.0	1.4	0.0
D2[1]	0.0	1.1	0.0	0.0	0.5
	0.1	1.1	0.0	0.0	0.5
PNF[2]	3.2	1.5	0.0	0.2	0.2
	3.6	0.8	0.0	0.0	0.1
PF[2]	0.4	3.6	0.0	0.3	0.5
	0.8	3.8	0.0	0.1	0.1
PW[2]	0.0	0.0	0.4	0.0	0.0
	0.0	0.0	0.4	0.0	0.0
D1[2]	0.2	0.8	0.0	0.3	0.0
	0.2	0.8	0.0	0.3	0.0
D2[2]	0.0	1.0	0.0	0.0	0.2
	0.0	1.0	0.0	0.0	0.2
PNF[3]	3.7	1.2	0.0	0.5	0.5
	3.4	0.3	0.0	0.1	0.1
PF[3]	0.6	2.9	0.0	0.2	0.0
	0.6	2.9	0.0	0.1	0.0
PW[3]	0.1	0.0	0.4	0.0	0.0
	0.1	0.0	0.4	0.0	0.0
D1[3]	0.2	0.2	0.0	0.3	0.0
	0.3	0.2	0.0	0.2	0.0
D2[3]	0.0	0.1	0.0	0.0	0.1
	0.0	0.1	0.0	0.0	0.1

Table 7
User's and producer's accuracy estimates for VCT (not shaded) and VCTw (shaded) representing the lower Lake Superior basin[1], upper Lake Michigan basin[2], and lower Lake Michigan basin[3].

	User's accuracy		Producer's accuracy	
	Estimate	SE	Estimate	SE
PNF[1]	95.9	2.2	42.1	8.6
	92.2	3.4	72.3	7.4
PF[1]	82.8	2.4	99.5	0.2
	85.4	2.6	98.9	0.4
PW[1]	100.0	0.0	91.2	6.2
	100.0	0.0	94.7	2.8
D1[1]	82.5	8.3	47.4	13.1
	93.5	3.3	46.5	13.0
D2[1]	52.5	14.5	37.9	10.6
	89.9	3.9	36.2	10.1
PNF[2]	91.9	2.4	74.9	4.9
	88.0	2.8	92.3	3.2
PF[2]	87.0	2.8	95.5	1.1
	91.8	2.0	94.6	1.3
PW[2]	99.4	0.7	97.3	2.3
	99.4	0.7	97.3	2.3
D1[2]	66.5	5.9	55.9	10.7
	83.3	3.1	55.9	10.7
D2[2]	60.7	12.0	49.0	11.6
	82.4	3.0	49.0	11.6
PNF[3]	96.0	1.2	86.9	2.2
	95.8	1.1	97.5	0.5
PF[3]	84.8	3.2	91.0	2.1
	96.2	1.2	91.1	1.9
PW[3]	99.9	0.1	94.9	3.5
	99.9	0.1	94.9	3.5
D1[3]	28.1	8.5	62.8	13.6
	45.7	8.6	47.8	11.6
D2[3]	17.7	4.6	85.5	11.5
	40.3	5.0	85.5	11.5

further, VCT, and hence VCTw, excels at detecting stand-clearing disturbances that remove all or most of the forest canopy but has difficulty consistently mapping partial canopy disturbances and/or tree defoliation (Huang et al., 2010a). As expected, VCTw successfully mapped some of the partial forest disturbances and excluded others, which created systematic inconsistencies in the validation procedures for D1 and D2. Post-accuracy assessment analysis identified multiple instances where a partial canopy disturbance was classified as the beginning year for a disturbance class that was not properly denoted by VCTw until the full canopy was removed. There were also additional scenarios where VCTw did not detect a partial canopy disturbance that appeared significant on aerial photography. Therefore, we suspect many of the disturbance class errors simply represent incongruities between manual and computerized interpretations of disturbances, and are ultimately overestimated. We did not refine manual interpretations of disturbances in order to maintain the integrity of an objective and unbiased accuracy assessment. Nevertheless, the suppressed accuracies of D1 and D2 remain statistically significant within the context of a complex sampling scheme containing thousands of points, indicating the proper coding of many disturbances.

Table 8
Differences between the overall accuracies of VCT and VCTw with the corresponding standard error (SE) and 95% confidence interval (CI).

	Difference	SE	CI
Entire study area	+4.89	0.89	3.14
			6.63
Lower Lake Superior basin	+4.09	1.49	1.47
			6.71
Upper Lake Michigan basin	+3.84	1.52	0.87
			6.81
Lower Lake Michigan basin	+6.62	1.34	3.71
			9.54

Most land cover products are used for conducting assessments of large geographic extents (e.g., the Great Lakes basins). Thus, it is not only the site-specific (per-pixel) accuracy that is important, but also the non-site specific accuracy of the resulting land area estimates. VCTw estimates of forest land area, unlike VCT, compared favorably with FIA's strategic forest inventory estimates for the two most heavily forested strata (LLSB, ULMB), adding validity to the approach of using VCTw to augment sample-based inventories with spatially explicit information on forest cover and forest disturbance. Compared with FIA, VCTw produced slightly higher estimates of forest land area in the LLMB, a stratum of sparse and fragmented forest cover. Causes of this deviation are not known, but could include one or more of the following: 1) definitional differences, for example, FIA's exclusion of some tree cover not defined as forest land use, 2) local misclassification of the input NLCD forest land cover class, resulting in incorrect assignment of training pixels in the VCT algorithm, and 3) inconsistent cover and quality of snow in the lowest latitudes of the study.

5. Conclusion

VCTw clearly outperformed VCT on a complex regional landscape of deciduous, mixed, and coniferous forests in the western Great Lakes to produce improved forest disturbance products. Similar VCTw and FIA-based estimates of forest land lend additional credence to the validity of the approach. VCTw also remains attractive from processing and application perspectives because it efficiently exploits only two seasons of imagery, as opposed to the three required seasons for NLCD. Furthermore, the LTSSw only require approximately quadrennial temporal frequency that consumes much less processing time than the approximately biennial LTSSs. VCTw ultimately relies upon hardware, software, algorithms, and data similar to the already extremely efficient VCT and only extends processing time about 2 h per path/row on a standard desktop computer. Indeed, VCTw appears poised to provide improved assessments of spatially explicit changes in forest and forest disturbances at landscape scales throughout geographic extents with adequate seasonal snow cover. This may provide crucial data-driven momentum encouraging abundant landscape ecological investigations (e.g., Stueve et al., 2011).

However, additional research remains necessary. For example, mapping snow with an internal VCTw algorithm originally designed to map clouds may not suffice in mountainous regions with complex topographic features and/or low winter sun angles. Financial constraints prevented us from experimenting with algorithms specifically designed for mapping snow, but these will be explored and incorporated in a future version of VCTw. It would also be beneficial to develop and improve techniques for constructing surrogate LTSSs and LTSSw from other remote sensing platforms where coverage from the Landsat archive is insufficient (e.g., as discussed by Huang et al., 2010a). This is particularly relevant for Landsat paths/rows in the northern reaches of the boreal forest, where there is a paucity of summer and especially winter Landsat coverage. If these obstacles can be surmounted, this novel approach has potential for widespread international applications and may be a worthwhile endeavor for the approximately 34% of the world's forest that receives sufficient snowfall to cover the ground, particularly the boreal and temperate forest with an estimated 100% and 70% snow coverage, respectively, during peak winter months (Fig. 12). The success of VCTw ultimately suggests the need for future research investigating the potential benefits of integrating multitemporal imagery from different seasons in automated disturbance mapping approaches.

Acknowledgements

The EPA, NASA Applied Science Program (via the NAFD project), USDA Forest Service Northern Research Station FIA Unit, and USDA Forest Service Remote Sensing Applications Center (RSAC) provided

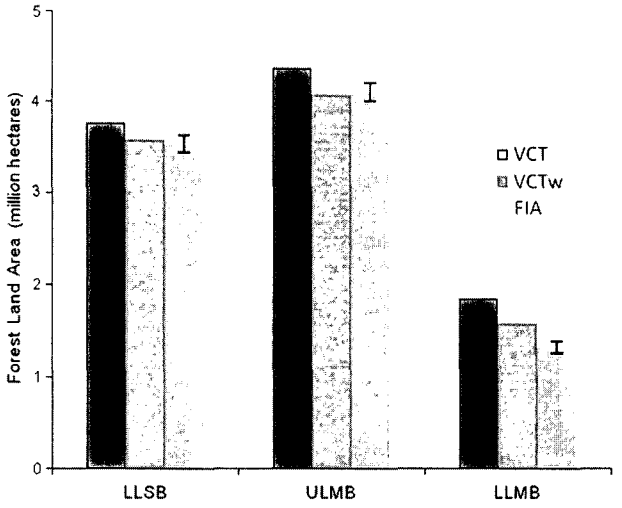

Fig. 11. Comparison of late period (2000–2008) estimates of forest land area from VCT, VCTw, and FIA (±95% confidence intervals), for lower Lake Superior basin (LLSB), upper Lake Michigan basin (ULMB), and lower Lake Michigan basin (LLMB), USA.

generous funding and support of this research. Mark Finco, Don Evans, Carl Albury, Greg Liknes, Sam Goward, and Nancy Thomas contributed invaluable critiques and assistance throughout various stages of the project. Kirk Stueve and Ian Housman envisioned the idea of using winter imagery to mitigate false positives. Kirk also wrote most of the paper, designed most figures and tables, and provided continual scientific support. Ian also spearheaded the implementation of the remote sensing methods at RSAC, provided input for all figures, performed the data analysis for Fig. 4, and contributed to the structure of the paper. Patrick Zimmerman led the design and implementation of the accuracy assessment. Patrick also contributed to writing the methods for the accuracy assessment, and supplied data for Fig. 10 and all of the tables. Mark Nelson provided substantive critical reviews of the manuscript and generated FIA-based estimates of forest area. Jeremy Webb contributed to the development of the winter imagery approach, created Figs. 2 and 5, led the interpretation of the validation

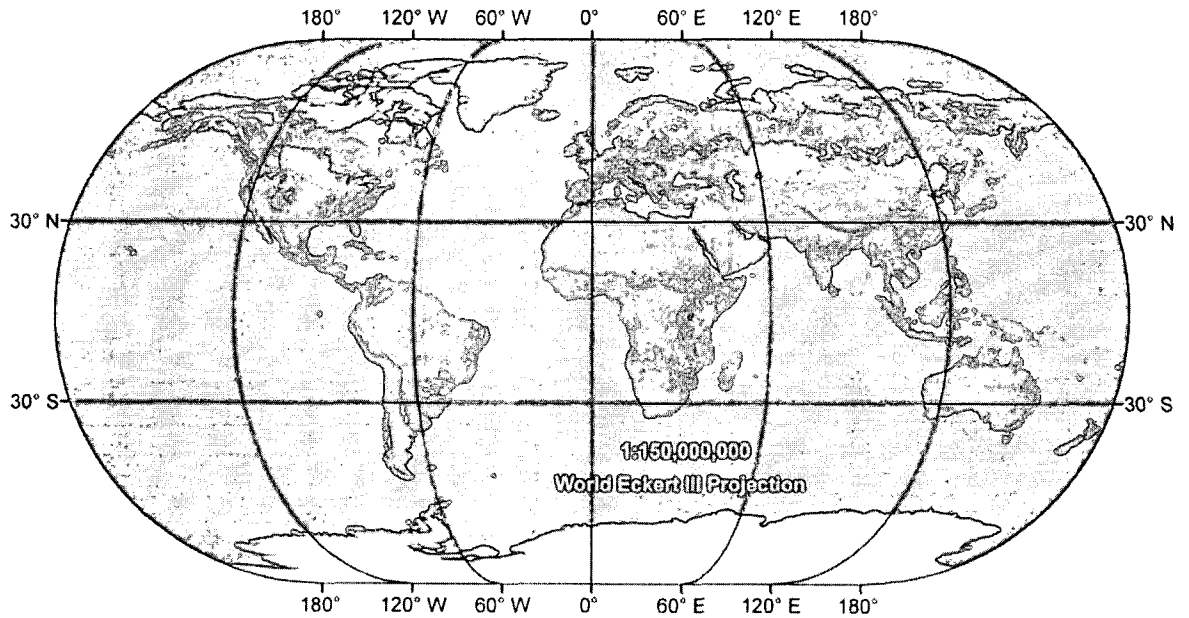

Ecological Zone	Global Coverage (%)	Snow (%)
Tropics	47	0
Boreal	33	100
Temperate	11	70
Subtropics	9	0
World Total	100	

Source: FAO 2001

Fig. 12. Estimated percent of the world's forest covered by snow and corresponding coverage in respective ecological zones, based on a 1-month composite map of 2002 snow cover during the peak winter months in the northern and southern hemispheres.

points, wrote part of the methods for the accuracy assessment, and provided support for making other figures. Hobie Perry provided overall management of the GLRI project, funding and contract support for the work conducted by RSAC, technical coordination and communication with research partners, critical feedback for several manuscript drafts, and scientific guidance. Robert Chastain provided remote sensing technical expertise at key stages and critiqued several manuscript drafts. Dale Gormanson designed the map in Fig. 12 and performed the global analyses of forest and snow cover. Chengquan Huang, Sean Healey, and Warren Cohen all provide a wealth of invaluable experience with multitemporal automated disturbance mapping and substantive feedback for several manuscript drafts. Two anonymous reviewers also gave invaluable advice for improving the paper.

References

Bailey, R. G., Avers, P. E., King, T., & McNab, W. H. (1994). Ecoregions and subregions of the United States. Map with supplementary table of map unit descriptions compiled and edited by W. H. McNab and R. G. Bailey. USDA Forest Service. Washington, D.C., USA.

Chuvieco, E., Ventura, G., Martín, M. P., & Gómez, I. (2005). Assessment of multitemporal compositing techniques of MODIS and AVHRR images for burned land mapping. *Remote Sensing of Environment, 94*, 450–462.

Cohen, W. B., & Goward, S. N. (2004). Landsat's role in ecological applications of remote sensing. *Bioscience, 54*(6), 535–545.

Cohen, W. B., Maiersperger, T. K., Yang, Z., Gower, S. T., Turner, D. P., Ritts, W. D., et al. (2003). Comparisons of land cover and LAI estimates derived from ETM+ and MODIS for four sites in North America: A quality assessment of 2000/2001 provisional MODIS products. *Remote Sensing of Environment, 88*(3), 233–255.

Cohen, W. B., Yang, Z., & Kennedy, R. (2010). Detecting trends in forest disturbance and recovery using yearly Landsat time series: 2. TimeSync—Tools for calibration and validation. *Remote Sensing of Environment, 114*(12), 2911–2924.

Costanza, R., d'Arge, R., de Groot, R., Farber, S., Grasso, M., Hannon, B., et al. (1997). The value of the world's ecosystem services and natural capital. *Nature, 387*, 253–260.

Dixon, R. K., Solomon, A. M., Brown, S., Houghton, R. A., Trexir, M. C., & Wisniewski, J. (1994). Carbon pools and flux of global forest ecosystems. *Science, 263*, 185–190.

Dozier, J. (1989). Spectral signature of alpine snow cover from the Landsat Thematic Mapper. *Remote Sensing of Environment, 28*, 9–22.

Duguay, C. R. (1995). An approach to the estimation of surface net radiation in mountain areas using remote sensing and digital terrain data. *Theoretical Applications in Climatology, 52*, 55–68.

Epting, J., Verbyla, D., & Sorbel, B. (2005). Evaluation of remotely sensed indices for assessing burn severity in interior Alaska using Landsat TM and ETM+. *Remote Sensing of Environment, 96*(3–4), 328–339.

Flatley, W. T., Lafon, C. W., & Grissino-Mayer, H. D. (2011). Climatic and topographic controls on patterns of fire in the southern and central Appalachian Mountains, USA. *Landscape Ecology, 26*, 195–209.

Foody, G. M. (2002). Status of land cover classification accuracy assessment. *Remote Sensing of Environment, 80*, 185–201.

Foster, D. R., Knight, D. H., & Franklin, J. F. (1998). Landscape patterns and legacies resulting from large, infrequent forest disturbances. *Ecosystems, 1*, 497–510.

Franco-Lopez, H., Ek, A. R., & Bauer, M. E. (2001). Estimation and mapping of forest stand density, volume, and cover type using the k-nearest neighbors method. *Remote Sensing of Environment, 77*, 251–274.

Goodale, C. L., Apps, M. J., Birdsey, R. A., Field, C. B., Heath, L. S., Houghton, R. A., et al. (2002). Forest carbon sinks in the northern hemisphere. *Ecological Applications, 12*(3), 891–899.

Goward, S. N., Arvidson, T. J., Faundeen, J., Williams, D. L., Irons, J., & Franks, S. (2006). Historical record of Landsat global coverage: Mission operations, NSLRSDA, and international cooperator stations. *Photogrammetric Engineering and Remote Sensing, 72*, 1155–1169.

Goward, S. N., Masek, J. G., Cohen, W. B., Moisen, G. G., Collatz, G. J., Healey, S. P., et al. (2008). Forest disturbance and North American carbon flux. *EOS Transactions, American Geophysical Union, 89*, 105–106.

Gustafsson, D., Lewan, E., & Jansson, P. (2004). Modeling water and heat balance of the boreal landscape—Comparison of forest and arable land in Scandinavia. *Journal of Applied Meteorology, 43*, 1750–1767.

Heath, L. S., Smith, J. E., Woodall, C. W., Azuma, D. L., & Waddell, K. L. (2011). Carbon stocks on forestland of the United States, with emphasis on USDA Forest Service ownership. *Ecosphere, 2*(1) art6..

Homer, C., Dewitz, J., Fry, J., Coan, M., Hossain, N., Larson, C., et al. (2007). Completion of the 2001 National Land Cover Database for the conterminous United States. *Photogrammetric Engineering and Remote Sensing, 73*, 337–341.

Homer, C., Huang, C., Yang, L., Wylie, B., & Coan, M. (2004). Development of a 2001 National Land-cover Database for the United States. *Photogrammetric Engineering and Remote Sensing, 70*, 829–840.

Huang, C., Goward, S. N., Masek, J. G., Gao, F., Vermote, E. F., Thomas, N., et al. (2009). Development of time series stacks of Landsat images for reconstructing forest disturbance history. *International Journal of Digital Earth, 2*, 195–218.

Huang, C., Goward, S. N., Masek, J. G., Thomas, N., Zhu, Z., & Vogelmann, J. E. (2010a). An automated approach for reconstructing recent forest disturbance history using dense Landsat time series stacks. *Remote Sensing of Environment, 114*, 183–198.

Huang, C., Thomas, N., Goward, S. N., Masek, J. G., Zhu, Z., Townshend, J. R. G., et al. (2010b). Automated masking of cloud and cloud shadow for forest change analysis using Landsat images. *International Journal of Remote Sensing, 31*, 5449–5464.

Jakubauskas, M. E. (1996). Thematic mapper characterization of lodgepole pine seral stages in Yellowstone National Park, USA. *Remote Sensing of Environment, 56*(2), 118–132.

Jin, S., & Sader, S. A. (2005). MODIS time-series imagery for forest disturbance detection and quantification of patch size effects. *Remote Sensing of Environment, 99*, 462–470.

Kennedy, R. E., Cohen, W. B., & Schroeder, T. A. (2007). Trajectory-based change detection for automated characterization of forest disturbance dynamics. *Remote Sensing of Environment, 110*, 370–386.

Kennedy, R. E., Yang, Z., & Cohen, W. B. (2010). Detecting trends in forest disturbance and recovery using yearly Landsat time series: 1. LandTrendr—Temporal segmentation algorithms. *Remote Sensing of Environment, 114*, 2897–2910.

Kittredge, D. B., Jr., Finley, A. O., & Foster, D. R. (2003). Timber harvesting as ongoing disturbance in a landscape of diverse ownership. *Forest Ecology and Management, 180*(1–3), 425–442.

Kurz, W. A., Dymond, C. C., Stinson, G., Rampley, G. J., Neilson, E. T., Carroll, A. L., et al. (2008). Mountain pine beetle and forest carbon feedback to climate change. *Nature, 452*, 987–990.

Lambin, E. F. (1996). Change detection at multiple temporal scales: Seasonal and annual variations in landscape variables. *Photogrammetric Engineering and Remote Sensing, 62*(8), 931–938.

Lu, D., Mausel, P., Brondízio, E., & Moran, E. (2004). Change detection techniques. *International Journal of Remote Sensing, 25*, 2365–2401.

Lumley, T. (2004). Analysis of complex survey samples. *Journal of Statistical Software, 9*(1), 1–19.

Lumley, T. (2010). *Survey: Analysis of complex survey samples.* R package version 3.23-3.

Millward, A. A., Warren, D. R., & Kraft, C. E. (2010). Ice storm damage greater along the terrestrial–aquatic interface in forested landscapes. *Ecosystems, 13*, 249–260.

Myers, N., Mittermeier, R. A., Mittermeier, C. G., da Fonseca, G. A. B., & Kent, J. (2000). Biodiversity hotspots for conservation priorities. *Nature, 403*, 853–858.

Nelson, M. D., Healey, S. P., Moser, K. W., & Hansen, M. H. (2009). Combining satellite imagery with forest inventory data to assess damage severity following a major blowdown event in northern Minnesota, USA. *International Journal of Remote Sensing, 30*, 5089–5108.

Nusser, S. M., & Klaas, E. E. (2003). Survey methods for assessing land cover map accuracy. *Environmental and Ecological Statistics, 10*(3), 309–331.

Odenweller, J. B., & Johnson, K. I. (1984). Crop identification using Landsat temporal-spectral profiles. *Remote Sensing of Environment, 14*, 39–54.

Olson, D. M., Dinerstein, E., Wikramanayake, E. D., Burgess, N. D., Powell, G. V. N., Underwood, E. C., et al. (2001). Terrestrial ecoregions of the world: A new map of life on earth. *Bioscience, 51*(11), 933–938.

Ozesmi, S. L., & Bauer, M. E. (2002). Satellite remote sensing of wetlands. *Wetlands Ecology and Management, 10*, 381–402.

Radeloff, V. C., Hammer, R. B., & Stewart, S. I. (2005). Rural and suburban sprawl in the U.S. Midwest from 1940 to 2000 and its relation to forest fragmentation. *Conservation Biology, 19*, 793–805.

R Development Core Team, R. (2010). R: A language and environment for statistical computing. Vienna, Austria: R Foundation for Statistical Computing 3-900051-07-0 http://www.R-project.org/.

Rice, A. H., Pyle, E. H., Saleska, S. R., Hutyra, L., Palace, M., Keller, M., et al. (2004). Carbon balance and vegetation dynamics in an old-growth Amazonian forest. *Ecology, 14*, 55–71.

Rich, R. L., Frelich, L., Reich, P. B., & Bauer, M. E. (2010). Detecting wind disturbance severity and canopy heterogeneity in boreal forest by coupling high-spatial resolution satellite imagery and field data. *Remote Sensing of Environment, 114*(2), 299–308.

Rock, B. N., Vogelmann, J. E., Williams, D. L., Vogelmann, A. F., & Hoshizaki, T. (1986). Remote detection of forest damage. *Bioscience, 36*(7), 439–445.

Särndal, C. E., Swensson, B., & Wretman, J. (1992). *Model assisted survey sampling.* New York, USA: Springer-Verlag.

Schmiegelow, F. K. A., Stepnisky, D. P., Stambaugh, C. A., & Koivula, M. (2006). Reconciling salvage logging of boreal forests with a natural-disturbance management model. *Conservation Biology, 20*(4), 971–983.

Schulte, L. A., Mladenoff, D. J., Crow, T. R., Merrick, L. C., & Cleland, D. T. (2007). Homogenization of northern U.S. Great Lakes forests due to land use. *Landscape Ecology, 22*, 1089–1103.

Sicart, J. E., Pomeroy, J. W., Essery, R. L., Hardy, J., Link, T., & Marks, D. (2004). A sensitivity study of daytime net radiation during snowmelt to forest canopy and atmospheric conditions. *Journal of Hydrometeorology, 5*, 774–784.

Singh, A. (1989). Digital change detection techniques using remotely-sensed data. *International Journal of Remote Sensing, 10*, 989–1003.

Soverel, N. O., Perrakis, D. D. B., & Coops, N. C. (2010). Estimating burn severity from Landsat dNBR and RdNBR indices aross western Canada. *Remote Sensing of Environment, 114*(9), 1896–1909.

Stehman, S. V., Wickham, J. D., Smith, J. H., & Yang, L. (2003). Thematic accuracy of the 1992 National Land-Cover Data for the eastern United States: Statistical methodology and regional results. *Remote Sensing of Environment, 86*(4), 500–516.

Stueve, K. M., Cerney, D. L., Rochefort, R. M., & Kurth, L. L. (2009). Post-fire tree establishment patterns at the alpine treeline ecotone: Mount Rainier National Park, Washington, USA. *Journal of Vegetation Science, 20*, 107–120.

Stueve, K. M., Lafon, C. W., & Isaacs, R. E. (2007). Spatial patterns of ice storm disturbance on a forested landscape in the Appalachian Mountains, Virginia. *Area, 39*, 20–30.

Stueve, K. M., Perry, C. H., Nelson, M. D., Healey, S. P., Hill, A. D., Moisen, G. G., et al. (2011). Ecological importance of intermediate windstorms rivals large, infrequent disturbances in the northern Great Lakes. *Ecosphere, 2*(1) art2.

Suzuki, K., Kodama, Y., Yamazaki, T., Kosugi, K., & Nakai, Y. (2008). Snow accumulation on evergreen needle-leaved and deciduous broad-leaved trees. *Boreal Environment Research, 13*, 403–416.

Suzuki, K., Nakai, Y., Ohta, T., Nakamura, T., & Ohata, T. (2003). Effect of snow interception on the energy balance above deciduous and coniferous forests during a snowy winter. *Water Resources Systems, 280*, 309–317.

Thomas, N. E., Huang, C., Goward, S. N., Powell, S., Rishmawi, K., Schleeweis, K., et al. (2011). Validation of North American forest disturbance dynamics derived from Landsat time series stacks. *Remote Sensing of Environment, 115*, 19–32.

Turner, M. G. (2005). Landscape ecology: What is the state of the science? *Annual Review of Ecology, Evolution, and Systematics, 36*, 319–344.

Verbesselt, J., Hyndman, R., Newnham, G., & Culvenor, D. (2010). Detecting trend and seasonal changes in satellite image time series. *Remote Sensing of Environment, 114*(1), 106–115.

Vikhamar, D., & Solberg, R. (2003a). Snow-cover mapping in forests by constrained linear spectral unmixing of MOSIS data. *Remote Sensing of Environment, 88*(3), 309–323.

Vikhamar, D., & Solberg, R. (2003b). Subpixel mapping of snow cover in forests by optical remote sensing. *Remote Sensing of Environment, 84*(1), 69–82.

Vikhamar, D., Solberg, R., & Seidel, K. (2004). Reflectance modeling of snow-covered forests in hilly terrain. *Photogrammetric Engineering and Remote Sensing, 70*(9), 1069–1079.

Walterman, M., Finco, M., & Healey, S. P. (2008). *Improving local area accuracy in national level disturbance mapping* (pp. 1–9). RSAC-4027-RPT1.

Warren, S. G. (1982). Optical properties of snow. *Reviews of Geophysics and Space Physics, 20*(1), 67–89.

Wickham, J. D., Stehman, S. V., Smith, J. H., & Yang, L. (2004). Thematic accuracy of the 1992 National Land-Cover Data for the western United States. *Remote Sensing of Environment, 91*, 452–468.

Wolter, P. T., Johnston, C. A., & Niemi, G. J. (2006). Land use land cover change in the U.S. Great Lakes basin 1992 to 2001. *Journal of Great Lakes Research, 32*(3), 607–628.

Wolter, P. T., Mladenoff, D. J., Host, G. E., & Crow, T. R. (1995). Improved forest classification in the northern lake states using multi-temporal Landsat imagery. *Photogrammetric Engineering and Remote Sensing, 61*(9), 1129–1143.

Woods, K. D. (2004). Intermediate disturbance in a late-successional hemlock-northern hardwood forest. *Journal of Ecology, 92*, 464–476.

Zimmerman, P. L., Housman, I. W., Perry, C. H., Chastain, R. A., & Finco, M. V. in progress. An accuracy assessment of land cover change in the western Great Lakes.